# Counterion-Correlation-Induced Attraction and Necklace Formation in Polyelectrolyte Solutions: Theory and Simulations

**Qi Liao,[†] Andrey V. Dobrynin,*[,‡] and Michael Rubinstein[§]**

*State Key Laboratory of Polymer Physics and Chemistry, Joint Laboratory of Polymer Science and Materials, Institute of Chemistry, Chinese Academy of Sciences, Beijing 100080, China; Polymer Program, Institute of Materials Science and Department of Physics, University of Connecticut, Storrs, Connecticut 06269-3136; and Department of Chemistry, University of North Carolina, Chapel Hill, North Carolina 27599-3290*

*Received September 26, 2005; Revised Manuscript Received December 13, 2005*

ABSTRACT: We have developed a necklace model of hydrophobic polyelectrolytes in which the necklace structure consisting of polymeric globules (beads) connected by extended sections of the chain (strings of monomers) appears as a result of the counterion condensation and is caused by the balance of the correlation-induced attraction of condensed counterions to charged monomers and electrostatic repulsion between uncompensated charges. The size of the beads increases with polymer concentration while their number per chain decreases. We predict coexistence of necklaces with different number of beads on a polymer backbone at any polymer concentration. To test this necklace model, we performed molecular dynamics simulations of polyelectrolyte chains with degree of polymerization $N$ varying from 25 to 373 and with fraction of charged monomers $f = {}^1/_3$, ${}^1/_2$, and 1 in poor solvent conditions for polymer backbone. The observed concentration dependence of the bead size supports the assumption of the counterion condensation origin of the necklace structure. The overlap concentration is almost independent of the degree of polymerization for weakly charged chains ($f = {}^1/_3$). For strongly charged chains with $f = 1$ the overlap concentration follows the normal $N$ dependence observed for polyelectrolyte solutions in $\Theta$ and good solvent regimes for polymer backbone. In semidilute solutions the correlation length of fully charged chains is inversely proportional to the square root of polymer concentration. The osmotic coefficient of the solutions of polyelectrolytes in poor solvent conditions for polymer backbone exhibits nonmonotonic concentration dependence in agreement with two-zone model predictions. It decreases with increasing polymer concentration in dilute solutions, while it is an increasing function of polymer concentration in the semidilute regime. The Kratky plot of the chain form factor is in excellent agreement with the neutron scattering experiments.

## 1. Introduction

Polymers in poor solvents have negative second virial coefficient, corresponding to an effective attraction between monomers. This attraction causes neutral polymer chains without charged groups to collapse into spherical globules in order to maximize the number of favorable polymer−polymer contacts and to minimize the number of unfavorable polymer−solvent contacts.[1,2] Polymeric globules change their shape and size upon charging. This phenomenon was observed over 50 years ago by Katchalsky and Eisenberg[3] in their study of the viscosity of aqueous solutions of poly(methacrylic acid) (PMA). The viscosity of dilute PMA solutions stayed almost constant at low solution pH and then abruptly increased as solution pH reached some critical value, indicating a dramatic change in the chain dimensions. This dramatic change in solution viscosity of PMA is qualitatively different from the gradual increase of viscosity observed in solutions of poly(acrylic acid)[3] (PAA), indicating continuous expansion of polymer chains. The difference in the behavior of PMA and PAA is due to the fact that water is a poor solvent for PMA that has hydrophobic methyl groups, while it is a good solvent for PAA. (For a historic overview of this subject see the paper by Morawetz.[4])

An abrupt conformational transition of a polyelectrolyte chain in a poor solvent was observed in computer simulations by Hooper et al.[5] and by Higgs and Orland.[6] By performing lattice Monte Carlo simulations of polyelectrolytes with attractive segment−segment interactions, it was observed that these polymers undergo an abrupt transition from a collapsed to an extended conformation with increasing charge. As the strength of the segment−segment attraction decreases, the transition becomes less pronounced.[5] Thus, the shape of a charged polymer in a poor solvent is determined by the interplay between long-range electrostatic repulsion and short-range attraction. However, important questions remained unanswered in these studies: how does this transition depend on the degree of polymerization of the polyelectrolyte chain, and what are the conformations of a polymer chain before and after this transition?

It is interesting to point out that the problem of the shape of a charged globule is similar to the classical problem of the instability of a charged droplet, considered by Lord Rayleigh over 100 years ago.[7] In his classical experiments Rayleigh had shown that a charged droplet is unstable and breaks into smaller droplets if its charge exceeds some critical value. The value of the critical charge is controlled by the electrostatic energy, $Q^2/(\epsilon R)$, of the droplet of size $R$ with charge $Q$ and its surface energy $\gamma R^2$ where $\epsilon$ is the dielectric constant of the solvent and $\gamma$ is the surface tension of the air−water interface. Balancing these two energies, one finds that the critical charge $Q_{crit}$ scales with the size of the droplet as $R^{3/2}$. (For a charged droplet containing $N$ molecules with size $R \sim N^{1/3}$, the value of the critical charge $Q_{crit}$ is proportional to the square root of the number of molecules in the droplet, $Q_{crit} \sim N^{1/2}$.) The equilibrium state of the charged droplet with $Q > Q_{crit}$ is a set of smaller droplets with the charge on each of them smaller than the critical one and placed at infinite distance from each other.

[†] Chinese Academy of Sciences.
[‡] University of Connecticut.
[§] University of North Carolina.
* Corresponding author. E-mail: avd@ims.uconn.edu.

10.1021/ma052086s CCC: $33.50 
Published on Web 02/04/2006

Rayleigh's experiments give a hint to what happens with charged solvophobic polymers (polyelectrolytes) during the transition from a collapsed to an extended conformation. A polyelectrolyte chain in a poor solvent reduces its energy in a way similar to a charged droplet by splitting into a set of smaller charged globules, called beads. A number of monomers in each bead is determined by the Rayleigh's stability condition. Since these transformations occur in a single chain, all these beads are connected by strings of monomers into a necklace globule.[8] This necklace model of a polyelectrolyte chain in a poor solvent was proposed by Dobrynin, Rubinstein, and Obukhov.[8] To test the predictions of the necklace model, they have performed Monte Carlo simulations of a freely jointed uniformly charged polyelectrolyte chain with fractional charge $f$ on each monomer.[8] These simulations have shown that the critical charge $Q_{crit}$ on a chain at which the charged globule becomes unstable is proportional to $N^{1/2}$, where $N$ is the degree of polymerization of the polymer. The polyelectrolyte chain adopts a dumbbell conformation for the charge $Q$ on the chain a little higher than the critical value $Q_{crit}$. At still larger charge, the polymer forms a necklace with three beads joined by two strings. These simulations demonstrated that in poor solvents there is a cascade of transitions between necklaces with different number of beads with increasing charge on the chain. The results of Monte Carlo simulations are in excellent qualitative agreement with the predictions of the necklace model of a polyelectrolyte chain in a poor solvent.[8]

The effect of solvent quality and salt concentration on the cascade of transitions between necklace structures with different number of beads was later investigated by Monte Carlo[9] and by molecular dynamics simulations.[10] In these simulations the salt effect was taken into account through the Yukawa potential. The full domain of stability of necklace globules in the solvent quality/salt concentration plane was investigated by Chodanowski and Stoll.[9] With increasing salt concentration the necklaces transform into elliptical globules, and at very high salt concentrations, with completely screened electrostatic interactions, polyelectrolyte globules become spherical. These results of computer simulations are in good qualitative agreement with theoretical models[8,11−13] of a polyelectrolyte chain in a poor solvent.

The necklace structure of polyelectrolyte chains in poor solvents was also confirmed by SANS experiments[14] in dilute solutions of water/acetone mixtures of poly(methacryloylethyltrimethylammonium methyl sulfate), by NMR spectra[15] of semidilute solutions of poly(styrenesulfonic acid) (PSS), poly(methacrylic acid) (PMA), and poly(acrylic acid) (PAA) in water/methanol mixtures, and by AFM images of poly(2-vinylpyridine) and poly(methacryloyloxyethyldimethylbenzylammonium chloride) adsorbed at mica surfaces.[16,17]

The existence of different length scales (chain size, string length, and bead size) for a necklace globule manifests itself in the unique scaling laws in semidilute polyelectrolyte solutions.[18,19] The correlation length $\xi$ of the solution above the overlap concentration $c^*$ has ordinary polyelectrolyte concentration dependence $\xi \sim c^{-1/2}$ while there are many beads per correlation volume $\xi^3$ (string-controlled regime). The intrachain electrostatic interactions in semidilute solutions are screened at the length scale on the order of the correlation length $\xi$, and a polyelectrolyte chain can be viewed as a Gaussian chain with effective bond length on the order of the correlation length $\xi$. This leads to the gradual decrease of the chain size $R$ with polymer concentration $c$ as $c^{-1/4}$. The crossover to a new concentration regime (bead controlled regime) occurs for the concentration range where the correlation length $\xi$ of the solution is on the order of the string length $l_{str}$ between two neighboring beads.[18,19] Polyelectrolyte solution at higher polymer concentrations can be envisioned as a dilute solution of beads with correlation length $\xi$ decreasing with polymer concentration as $\xi \sim c^{-1/3}$. The chain size $R$ shows stronger concentration dependence, $R \sim c^{-1/3}$, in this regime. Finally, at polymer concentrations higher than the bead overlap concentration, the correlation length of the solution is that of concentrated polyelectrolyte solution. Polyelectrolyte chains expand in this concentration range, reaching the size of Gaussian coils. Thus, the size of a solvophobic polyelectrolyte chain in semidilute solutions exhibits a nonmonotonic dependence on polymer concentration.

Essafi[20] and Spitteri[21] identified different concentration regimes in semidilute aqueous solutions of partially sulfonated poly(styrenesulfonate). It was reported by Essafi[20] that the exponent $\alpha$ of the power law concentration dependence of correlation length $\xi(c) \sim c^{\alpha}$ varies with the degree of sulfonation. For example, this exponent was $\alpha = -0.38$ for 40% sulfonation throughout the whole semidilute regime while it was close to the classical value $\alpha = -0.5$ for the fully sulfonated samples. Similar observations were reported by Heitz et al.[22] for poly(methacrylic acid) in water as a function of its neutralization. The exponent $\alpha$ of the concentration dependence of the correlation length was found to change from $-0.43$ to $-0.31$ as the neutralization decreased from 0.95 to 0.09. Evidence of the intrachain correlation peak in the Kratky plot associated with the presence of beads was seen in the small-angle neutron scattering experiments of Spitteri.[21] The evolution of the polyelectrolyte solution with increasing polymer concentration in solvophobic polyelectrolytes in a series of polar organic solvents[23] shows that the scaling exponent $\alpha$ of the concentration dependence of the correlation length changes from $-0.45$ to $-0.13$.

Molecular dynamics simulations of partially charged polyelectrolytes with explicit counterions in poor solvent conditions were performed by the Mainz group.[24−29] These simulations have shown that polyelectrolyte chains at low polymer concentrations form necklaces of beads connected by strings. The fraction of condensed counterions on the chain increases with increasing polymer concentration causing chain size to decrease by decreasing the length of strings and the number of beads per chain. At higher polymer concentrations polymer chains interpenetrate leading to a concentrated polyelectrolyte solution. In this range of polymer concentrations the chain size is observed to increase toward its Gaussian value. The nonmonotonic dependence of the chain size on polymer concentration is in qualitative agreement with theoretical predictions.[19] A comprehensive study of the effect of the short-range attractive and of the long-range electrostatic interactions on the necklace formation in dilute polyelectrolyte solutions was carried out by Limbach and Holm.[26−29] They have found that polyelectrolyte chains adopt necklace-like conformation only in the narrow range of the interaction parameters. At finite polymer concentrations the necklace stability region is strongly influenced by the counterion condensation. A similar trend was observed in Monte Carlo simulations of titration of hydrophobic polyelectrolytes by Ulrich et al.[30] Depending on the solvent quality for polymer backbone and pH−p$K_0$ value, a polyelectrolyte chain could be in five different conformational states: coil, collapsed spherical globule, necklace globule, sausage-like aggregate, and fully stretched chain.

The effect of counterions in the necklace model was studied analytically by Dobrynin and Rubinstein.[19] In the framework of the two-zone models for counterion condensation,[31] they have calculated the renormalization of the effective fraction of the ionized groups on the polymer backbone with increasing polymer concentration. In this approach the condensed (localized) counterions contribute only to the reduction of electrostatic repulsion between uncompensated charges, lowering the net electrostatic energy of the necklace. Thus, in this model the counterion condensation is due to a fine interplay between the reduction of electrostatic repulsion between uncompensated charges and the loss of the translational entropy by condensed counterions due to their localization in the vicinity of the polymer backbone. In a very dilute polyelectrolyte solution the entropic penalty for counterion localization is very high, and almost all counterions leave the polymer chain and stay in solution. However, as polymer concentration increases, the entropic penalty for counterion localization decreases, resulting in an increase in the number of condensed counterions. This model predicts that beads grow in size with increasing polymer concentration, while their number per chain decreases and polyelectrolyte chain shrinks.

While the necklace model with counterion condensation[19] provides a qualitative explanation of the simulation results,[24−27] it underestimates the effect of counterion condensation on chain conformations. In addition to the reduction of the chain charge, the simulation seems to indicate an additional contribution resulting in stronger chain collapse. There are two different mechanisms that could lead to effective attractive interactions induced by condensed counterions. The first one is the formation of permanent or relatively long-lived ionic pairs between condensed counterions and oppositely charged monomers. In this case dipole−dipole interactions between ion pairs result in additional attraction between monomers. These extra attractive interactions decrease the second virial coefficient, shifting the position of the $\theta$-temperature. The shift of the $\theta$-temperature in the case of strongly charge polyelectrolytes could be significant, leading to stronger chain collapse. A detailed analysis of the effect of the counterion condensation on the chain conformations in different temperature regimes was presented by Schiessel and Pincus[32] and by Schiessel.[33] However, the existence of permanent or long-living dipoles is not supported by computer simulations in the relevant range of parameters. In fact, counterions are highly mobile even when they are localized near the polymer backbones.

Another effect that can give rise to attractive interactions is the correlation-induced attraction between condensed counterions and charged monomers. These interactions are due to electrostatic attraction of a condensed counterion to a surrounding charged background consisting of charged monomers and other condensed counterions. In the case of weak electrostatic attraction the origin of these interactions is similar to the fluctuation-induced attraction in two-component plasma and is due to local charge density fluctuations. In the case of strong interactions this effect is due to correlation-induced attraction between counterions and oppositely charged background (similar to the interactions in strongly correlated Wigner liquid[34,35]). In the present paper we propose a necklace model based on the correlation-induced attraction between condensed counterions and charged monomers and test the predictions of this new necklace model by molecular dynamics simulations of polyelectrolytes in a poor solvent. In particular, we focus upon the concentration dependence of the size and the number of monomers in beads and strings as well as on the effects of the counterion condensation on chain structure. The rest of the paper is organized as follows. In section 2 we introduce a modified necklace model that is based on the counterion condensation and utilizes the correlation effects between condensed counterions. The simulation model and the algorithms are described in section 3, which also provides a detailed account of the simulation results for the end-to-end distance, overlap concentration, and correlation length in dilute and semidilute solutions. Finally, in section 4 we summarize our results.

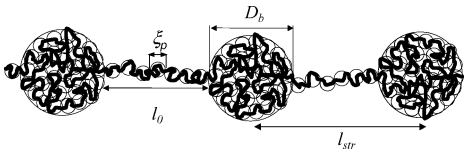


**Figure 1.** Schematic picture of a necklace formed by a partially charged polyelectrolyte chain in a poor solvent.

## 2. Necklace Globule Formed by Counterion-Correlation-Induced Attraction

**2.1. Necklace Globule.** Consider a necklace-like polyelectrolyte chain with the degree of polymerization $N$ and the fraction of charged monomers $f$ in a poor solvent. Let us assume that the necklace has $n_b$ beads of size $D_b$ with $m_b$ monomers in each. These beads are connected by strings each having $m_{str}$ monomers. (See Figure 1 for the definition of the different length scales.) The fraction $x$ of counterions is condensed inside beads (not shown in the figure). The beads are globules with the number density of monomers $\rho \approx m_b/D_b^3$. There are two different types of interactions inside a bead: short-range interactions between monomers and electrostatic interactions between charged monomers and counterions. The short-range interactions can be approximated by a virial expansion in the power series of monomer density $\rho$ [36]

$$\frac{F_b^{sh}}{k_B T} \approx m_b b^3 \tau \rho + m_b b^6 \rho^2 \tag{1}$$

where $\tau = 1 - \theta/T$ is the effective temperature and $\theta$ is the theta temperature, $k_B$ is the Boltzmann constant, and $T$ is the absolute temperature. In this section the analysis of the necklace globule is done on the scaling level, neglecting all numerical coefficients. At the $\theta$-temperature, the second virial coefficient is equal to zero, and the first term in eq 1 vanishes. Below the $\theta$-temperature, the first term is negative that corresponds to the poor solvent conditions for the polymer backbone.

The electrostatic interactions inside a bead can be represented as a sum of the electrostatic repulsion between charged monomers ($fm_b$ per bead), electrostatic attraction between charged monomers and condensed counterions ($xfm_b$ per bead), and electrostatic repulsion between condensed counterions

$$\frac{U_{electr}}{k_B T} \approx \frac{l_B (f m_b)^2}{D_b} - 2\frac{l_B x (f m_b)^2}{D_b} + \left\langle \frac{U_{cc}}{k_B T} \right\rangle_{count} \tag{2}$$

where the brackets $\langle \rangle_{count}$ denote averaging over distributions of counterions inside the bead. The Bjerrum length

$$l_B = e^2/(\epsilon k_B T) \tag{3}$$

determines the strength of the electrostatic interactions between two elementary charges $e$ in the medium with dielectric constant $\epsilon$. In writing eq 2, we have assumed that the charged monomers are uniformly distributed over the bead volume. We can rewrite

eq 2 by adding and subtracting the electrostatic repulsion between condensed counterions uniformly distributed over the bead volume with average density $xf\rho$. After this transformation the electrostatic energy of a bead is rewritten as follows:

$$\frac{U_{\text{electr}}}{k_{\text{B}}T} \approx \frac{l_{\text{B}}[(1-x)fm_{\text{b}}]^2}{D_{\text{b}}} + \left\langle \frac{U_{\text{cc}}}{k_{\text{B}}T} \right\rangle_{\text{count}} - \frac{l_{\text{B}}(xfm_{\text{b}})^2}{D_{\text{b}}} \quad (4)$$

The first term describes the electrostatic repulsion of the uniformly charged bead with the effective charge $(1-x)fm_b$. The last two terms in the eq 4 represent electrostatic interactions between condensed counterions and oppositely charged neutralizing background with charge density $xf\rho$. This part of the bead electrostatic energy is conventionally referred to as correlation part of the one component plasma (OCP) (see for details refs 34, 35, 37, and 38). The averaging of electrostatic interactions between condensed counterions and neutralizing background results in an additional correlation-induced attractive contribution to the bead electrostatic energy.

In a globule with polymer density $\rho$, condensed counterions are separated by a typical distance

$$\xi_{\text{c}} \approx (xf\rho)^{-1/3} \quad (5)$$

The correlation-induced attraction between counterions can be estimated as electrostatic attraction of a counterion and the oppositely charged neutralizing background with the effective charge density $xf\rho$ inside radius $\xi_c$. This leads to the correlation-induced attraction to be on the order of

$$\varphi_{\text{cor}} \approx -k_{\text{B}}Tl_{\text{B}}/\xi_{\text{c}} \quad (6)$$

per condensed counterion. In the above estimate of the correlation-induced attraction we use the strong correlation approximation for the OCP in which the interaction parameter $l_B/\xi_c$ is large, $l_B/\xi_c \geq 1$. In the case of weak interactions, $l_B/\xi_c \ll 1$, the attraction energy between a counterion and neutralizing background has a well-known Debye−Huckel form

$$\varphi_{\text{cor}} \approx -k_{\text{B}}T(l_{\text{B}}/\xi_{\text{c}})^{3/2} \quad (7)$$

In this section we will discuss necklace structure induced by condensed counterions both in the strongly correlated counterion approximation, $l_B/\xi_c \geq 1$, and in the weakly correlated counterion approximation, $l_B/\xi_c \ll 1$. The correlation-induced attractive interaction energy between counterions and neutralizing background in a bead is equal to[38]

$$\frac{U_{\text{OCP}}}{k_{\text{B}}T} \approx \left\langle \frac{U_{\text{cc}}}{k_{\text{B}}T} \right\rangle - \frac{l_{\text{B}}(xfm_{\text{b}})^2}{D_{\text{b}}} \approx m_{\text{b}}xf\varphi_{\text{cor}} \approx -m_{\text{b}}xf\begin{cases} l_{\text{B}}/\xi_{\text{c}}, & \text{for } \xi_{\text{c}} \leq l_{\text{B}} \\ (l_{\text{B}}/\xi_{\text{c}})^{3/2}, & \text{for } \xi_{\text{c}} \gg l_{\text{B}} \end{cases} \quad (8)$$

The total electrostatic energy of a bead with condensed counterions is the sum of repulsive (eq 2) and attractive (eq 8) terms

$$\frac{F_{\text{b}}^{\text{elec}}}{k_{\text{B}}T} \approx \frac{l_{\text{B}}[(1-x)fm_{\text{b}}]^2}{D_{\text{b}}} + m_{\text{b}}xf\frac{\varphi_{\text{cor}}}{k_{\text{B}}T} \quad (9)$$

The bulk energy of a bead includes both short-range (eq 1) and electrostatic (eq 9) energy contributions

$$\frac{F_{\text{b}}^{\text{bulk}}}{k_{\text{B}}T} \approx \frac{l_{\text{B}}[(1-x)fm_{\text{b}}]^2}{D_{\text{b}}} + m_{\text{b}}(\tau b^3\rho + b^6\rho^2 + xf\varphi_{\text{cor}}/k_{\text{B}}T) \quad (10)$$

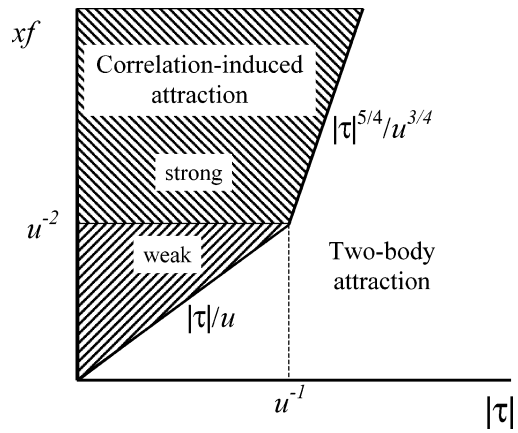


**Figure 2.** Diagram of different collapse mechanisms. Shaded area corresponds to correlation-induced attraction mechanisms of bead collapse (logarithmic scales).

The equilibrium polymer density inside a bead is obtained by minimizing the terms in the parentheses on the right-hand side of eq 10 with respect to polymer density $\rho$. The balance of the first two terms in parentheses results in the classical expression for the density inside a polymeric globule,[36] $\rho \approx b^{-3}|\tau|$, the collapse of which is induced by the two-body attractive interactions. Below we focus on another limiting case with attraction dominated by condensed counterions. In this case the equilibrium density inside a bead is determined by the balance of the second and the third terms in the parentheses on the right-hand side of eq 10. This results in the following expression for the polymer density inside a bead

$$\rho b^3 \approx \begin{cases} u^{3/5}(xf)^{4/5}, & \text{strongly correlated} \\ uxf, & \text{weakly correlated} \end{cases} \quad (11)$$

where $u$ is the ratio of the Bjerrum length $l_B$ to the bond size $b$, $u = l_B/b$. The first regime in eq 11 corresponds to the case of strong correlations between counterions with interaction parameter, $l_B/\xi_c \geq 1$. In this regime the correlation-induced attraction dominates over the two-body attraction if the fraction of condensed counterions $xf$ is larger than $u^{-3/4}|\tau|^{5/4}$ (see Figure 2). The second regime in eq 11 corresponds to weakly correlated condensed counterions, $l_B/\xi_c \ll 1$. The boundaries of this regime are $xf \approx u^{-2}$and $xf \approx |\tau|/u$, where the first condition determines the crossover between weakly and strongly correlated condensed counterions regimes ($\xi_c \approx l_B$) and the second boundary condition corresponds to crossover to the regime in which the globule is collapsed primarily by the two-body attraction. Figure 2 summarizes regimes with different bead collapse mechanisms. In the range of parameters $xf < |\tau|/u$ and $xf < u^{-3/4}|\tau|^{5/4}$ the equilibrium polymer density inside the bead is determined by balancing two- and three-body interactions. This leads to the usual necklace structure discussed in ref 8. However, for the interval of parameters $xf > |\tau|/u$ and $xf > u^{-3/4}|\tau|^{5/4}$ the bead collapse is due to the correlation-induced attraction.

The polymer density fluctuations inside the bead with polymer density $\rho$ given by eq 11 occur at the length scales smaller than the correlation length $\xi_p$. At these length scales the chain conformations are unperturbed by the polymer−counterion

attractive interactions and are those of an ideal chain of $g_p$ monomers ($\xi_p \approx b g_p^{1/2}$). At the length scales larger than the correlation blob size $\xi_p$, the three-body repulsion between monomers suppresses the polymer density fluctuations and correlation blobs in a bead are densely packed, $\rho \approx g_p/\xi_p^3$. Thus, the number of monomers in a correlation blob is

$$g_p \approx \begin{cases} u^{-6/5}(xf)^{-8/5}, & \text{strongly correlated} \\ (uxf)^{-2}, & \text{weakly correlated} \end{cases} \quad (12)$$

and its size is

$$\xi_p \approx b\begin{cases} u^{-3/5}(xf)^{-4/5}, & \text{strongly correlated} \\ (uxf)^{-1}, & \text{weakly correlated} \end{cases} \quad (13)$$

The average distance between condensed counterions inside a bead with polymer density $\rho$ is equal to

$$\xi_c \approx (xf\rho)^{-1/3} \approx b\begin{cases} u^{-1/5}(xf)^{-3/5}, & \text{strongly correlated} \\ u^{-1/3}(xf)^{-2/3}, & \text{weakly correlated} \end{cases} \quad (14)$$

In the case of strongly correlated counterions, $l_B/\xi_c \geq 1$, the distance between condensed counterions $\xi_c$ is larger than polymeric correlation length $\xi_p$. In this case the counterions interact with almost nonfluctuating charged polymeric neutralizing background. In the case of weakly correlated condensed counterions, $l_B/\xi_c \ll 1$, there are many condensed counterion per each polymeric correlation length $\xi_p > \xi_c$. Thus, fluctuations of both counterions and polymeric neutralizing background result in correlation (fluctuation)-induced attractive interactions. The polymeric correlation length $\xi_p$ in the case of the weakly correlated condensed counterion system is on the order of the Debye screening length $r_D$ due to condensed counterions $\xi_p \approx r_D \approx (l_b x f \rho)^{-1/2} \approx b(uxf)^{-1}$ (see eq 13), and both charge and polymer density fluctuations occur on the same length scale.

The size of a bead with polymer density $\rho$ and number of monomers $m_b$ is equal to

$$D_b \approx \xi_p (m_b/g_p)^{1/3} \approx b m_b^{1/3}\begin{cases} u^{-1/5}(xf)^{-4/15}, & \text{strongly correlated} \\ (uxf)^{-1/3}, & \text{weakly correlated} \end{cases} \quad (15)$$

The bulk free energy of a bead with equilibrium density $\rho$ given by eq 11 is on the order of

$$\frac{F_b^{bulk}(m_b)}{k_B T} \approx \frac{l_B[(1-x)f]^2 g_p^{1/3}}{\xi_p} m_b^{5/3} - m_b/g_p \quad (16)$$

The last term on the right-hand side of eq 16 can be considered as the number of monomers in a bead, $m_b$, times the chemical potential of a monomer inside the bead and represents the effective correlation-induced attractive interactions between monomers. This energy contribution is on the order of the thermal energy $k_B T$ per each polymeric correlation blob inside the bead. In addition to this bulk contribution to the free energy of beads, there is also a surface energy contribution. The origin of the surface energy is the difference in the number of the nearest neighbors for the condensed counterions at the surface of the bead and for the counterions inside the bead. It requires extra energy to bring a counterion to the surface from the bulk of the bead. The surface energy of a bead can be estimated for the strongly correlated case as the number of condensed counterions at the bead surface $(D_b/\xi_c)^2$ times the energy of electrostatic interaction between a counterion and the neutralizing background $k_B T l_B/\xi_c$

$$F_{surf} \approx k_B T \frac{D_b^2 l_B}{\xi_c^3} \approx k_B T \gamma m_b^{2/3}$$

where we have substituted the expression for the beads size $D_b$ (eq 15) and introduced dimensionless parameter $\gamma \approx u^{6/5}(xf)^{19/15}$. The surface energy of a bead in the weakly correlated case is $k_B T$ per correlation blob of size $\xi_p$ at the surface. There are $(m_p/g_p)^{2/3}$ such blobs per bead. Therefore, the surface energy can be written as

$$F_{surf} \approx k_B T \left(\frac{m_b}{g_p}\right)^{2/3} \approx k_B T \gamma m_b^{2/3}$$

where dimensionless parameter $\gamma \approx g_p^{-2/3}$. Thus, surface free energy in both strongly correlated and weakly correlated cases is written in the same form

$$F_{surf} \approx k_B T \gamma m_b^{2/3} \quad (17)$$

with dimensionless parameter

$$\gamma \approx \begin{cases} u^{6/5}(xf)^{19/15}, & \text{strongly correlated} \\ (uxf)^{4/3}, & \text{weakly correlated} \end{cases} \quad (18)$$

The total contribution to the necklace free energy from the surface free energy of beads is equal to the number of beads $n_b$ per chain times the surface energy of a bead given by eq 17.

The beads are connected by strings of monomers. Pulling monomers into a string requires extra energy $k_B T/g_p$ per monomer that is the difference between the average interaction energy of a monomer in a string and that in the interior (or even at the surface) of a bead. Thus, each string has an additional positive contribution to the necklace free energy due to the loss of favorable attractive interactions between charged monomers and condensed counterions. This is an analogue of the string surface energy term.

$$\frac{F_{str}^{surf}}{k_B T} \approx (n_b - 1) m_{str}/g_p \approx (n_b - 1) m_{str}\begin{cases} u^{6/5}(xf)^{8/5}, & \text{strongly correlated} \\ (uxf)^2, & \text{weakly correlated} \end{cases} \quad (19)$$

In addition to the surface free energy term, the free energy of a string has an elastic contribution due to the stretching of polymer backbone between beads. Combining elastic and surface free energy contributions, we can write the string free energy as

$$\frac{F_{str}}{k_B T} \approx (n_b - 1)\left(\frac{l_0^2}{b^2 m_{str}} + \frac{m_{str}}{g_p}\right) \quad (20)$$

where $l_0$ is the length of a strand with $m_{str}$ monomers (see Figure 1). Minimization of eq 20 with respect to $m_{str}$ at fixed length of a strand $l_0$ results in the relation connecting the distance between the surfaces of the two neighboring beads and the number of monomers in a string $m_{str}$.

$$m_{str} \approx g_p^{1/2} \frac{l_0}{b} \approx \frac{l_0}{b}\begin{cases} u^{-3/5}(xf)^{-4/5}, & \text{strongly correlated} \\ (uxf)^{-1}, & \text{weakly correlated} \end{cases} \quad (21)$$

A string can be viewed as a stretched array of polymeric

correlation blobs of size $\xi_p$. Substitution of the relation eq 20 into eq 21 leads to the linear dependence of the string's free energy on its length $l_0$

$$\frac{F_{str}}{k_BT} \approx (n_b - 1)\frac{l_0}{g_p^{1/2}b} \approx (n_b - 1)\frac{l_0}{b}\begin{cases} u^{3/5}(xf)^{4/5}, & \text{strongly correlated} \\ uxf, & \text{weakly correlated} \end{cases} \quad (22)$$

The electrostatic contribution to the necklace free energy includes the electrostatic energy of beads, electrostatic interaction between beads, electrostatic energy of strings, and electrostatic interaction between charged monomers and counterions. We have already evaluated the electrostatic energy of a bead, and its contribution was included into the free energy of a bead (eq 16). At the distances from the center of the bead on the order of half of the distance between beads $l_{str}/2$ the distribution of the electrostatic potential has cylindrical symmetry. The presence of counterions within the cylindrical volume with radius $l_{str}/2$ and total length $n_b l_{str}$ leads to the reduction of the bare charge on the necklace. Thus, the strength of the electrostatic repulsion between two neighboring beads responsible for the stretching of the string is controlled by the effective charge $Q_{eff}$ that is equal to the sum of the charge of the bead and charge of the string minus the charge of the counterions occupying volume $\sim l_{str}^3$ near the chain. Taking this fact into account, one can estimate the energy of electrostatic interactions between all beads on a chain and all counterions within a cylindrical region as the electrostatic energy of the cylinder of length $(n_b - 1)l_{str}$, diameter $l_{str}$ with the linear charge density $eQ_{eff}/l_{str}$

$$\frac{U_{neck}^{elec}}{k_BT} \approx \frac{l_B Q_{eff}^2}{l_{str}} \frac{n_b^2}{\sqrt{n_b^2 - 1}} \ln(n_b + \sqrt{n_b^2 - 1}) \quad (23)$$

The contribution to the electrostatic energy of a necklace from the spherical shell starting at the length scales on the order of the necklace length and continuing up to the distance between chains is smaller than the contributions from beads and cylindrical region and can be neglected in a dilute solution.

The total energy of a necklace can be written as a function of the number of monomers in a bead $m_b$, the number of beads on the chain $n_b$, and the string length

$$\frac{F_{neck}}{k_BT} \approx \frac{l_B Q_{eff}^2}{l_{str}} \frac{n_b^2}{\sqrt{n_b^2 - 1}} \ln(n_b + \sqrt{n_b^2 - 1}) + (n_b - 1)\frac{l_0}{g_p^{1/2}b} + n_b m_b\{\gamma m_b^{-1/3} + u[(1 - x)f]^2 g_p^{-1/6} m_b^{2/3}\} - N/g_p \quad (24)$$

The first term in eq 24 describes the electrostatic repulsion between beads, the second term is the surface energy of the strings, the two terms in the curly brackets correspond to the surface energy of all beads and their electrostatic self-energy, and finally the last term is the bulk free energy of the correlation-induced attraction between counterions and monomers. Equation 24 has to be minimized with the constraint that the total number of monomers in beads $n_b m_b$ plus the number of monomers in all strings $(n_b - 1)m_{str}$ is equal to the degree of polymerization $N$.

The equilibrium number of monomers in a bead, $m_b^*$, is obtained by minimizing the free energy of a necklace with respect to $m_b$, leading to

$$m_b^* \approx \frac{x}{(1 - x)^2 f} \quad (25)$$

The dependence of the number of monomers in a bead on the fraction of condensed counterions $x$ has the same form in both weakly and strongly correlated limits. The number of monomers in a bead increases as the effective fraction of ionized charged groups $(1 - x)f$ decreases. Equation 25 is another form of the Raylegh's stability condition for a charged globule with the collapse caused by condensed counterions.

The string length $l_{str}$ is derived by minimizing the first two terms of the free energy of a necklace eq 24 with respect to $l_{str}$. It is important to point out that the string length $l_{str}$ and the length $l_0$ between surfaces of neighboring beads differ by the bead diameter $D_b$ ($l_{str} = l_0 + D_b$). A qualitative dependence of the string length on the fraction of condensed counterions $xf$ can be obtained by assuming that the magnitude of the effective charge $Q_{eff}$ is mainly controlled by the counterions condensed inside beads. Within this approximation the parameter $Q_{eff}$ is proportional to $(1 - x)fm_b$, and the string length is estimated as

$$l_{str} \approx bu^{1/2} g_p^{1/4} K(n_b) Q_{eff} \approx \frac{bK(n_b)}{(1 - x)f}\begin{cases} u^{1/5}(xf)^{3/5}, & \text{strongly correlated} \\ (xf)^{1/2}, & \text{weakly correlated} \end{cases} \quad (26)$$

where the function $K(n_b)$ is defined as

$$K(n_b) = \frac{n_b}{(n_b - 1)^{3/4}(n_b + 1)^{1/4}} \sqrt{\ln(n_b + \sqrt{n_b^2 - 1})} \quad (27)$$

In the case with the number of monomers in a bead much larger than the number of monomers in a string, $m_b/m_{str} \gg 1$, the number of beads $n_b$ per chain is approximately equal to $N/m_b$. Since most of the length of the necklace is stored in the strings, this necklace length can be estimated as the number of strings $n_b - 1$ on the chain times the distance between the centers of mass of two neighboring beads $l_{str}$

$$R_e \approx (n_b - 1)l_{str} \approx b(1 - x)fNK(n_b)\begin{cases} u^{1/5}(xf)^{-2/5}, & \text{strongly correlated} \\ (xf)^{-1/2}, & \text{weakly correlated} \end{cases} \quad (28)$$

It is interesting to point out that in the case of weak fluctuation-induced attraction the equilibrium characteristics of the necklace globule such as the number of monomers in a bead, the bead size, and the string length are identical to those obtained for the necklace globule formed by a polyampholyte chain[39] if one substitutes the polyampholyte charge asymmetry $\delta f$ by the effective fraction of charged monomers $(1 - x)f$ and the total fraction of charged monomers $(f_+ + f_-)$ of polyampholyte by the fraction of condensed counterions $xf$ on polyelectrolyte beads.

Figure 3 shows a diagram of states of a polyelectrolyte chain as a function of the effective fraction of charged monomers $\Delta f = (1 - x)f$ and the fraction of condensed counterions $fx$ covering the range $|\tau|/u \le xf$. The correlation-induced attractive interactions between charged monomers and condensed counterions are stronger than two-body monomer−monomer attraction and drive chain collapse in this range of parameters (see Figure 2). The vertical dashed line $xf \approx u^{-2}$ in Figure 3 separates weakly and strongly correlated OCP regimes. There are three different

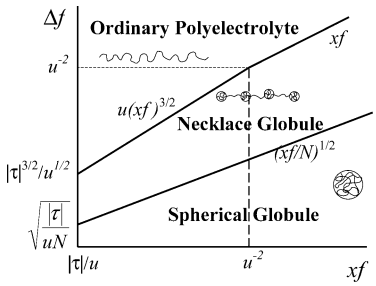


**Figure 3.** Diagram of states of a polyelectrolyte chain in a dilute solution in the parameter space of the fraction of the condensed counterions $xf$ and the effective fraction of ionized groups $\Delta f = (1 - x)f$ (logarithmic scales).

regions in the diagram of states. In the case of strong counterion condensation with large $xf$ the polyelectrolyte chain forms a spherical globule. The upper boundary for this regime is given by $\Delta f \approx (xf/N)^{1/2}$ and is obtained from the Rayleigh stability condition eq 25 by substituting $N$ for the number of monomers in a bead. In the case of small fraction of condensed counterions the polyelectrolyte chain forms a necklace globule with large beads and long strings. The increase of the effective fraction of charged monomers $\Delta f$ in this regime leads to the decrease of the bead size and at the same time to the decrease in the length of the string connecting beads. The size of beads decreases and thus the number of beads per chain increases with increasing $\Delta f$.

There is one condensed counterion per each bead when the bead size $D_b$ becomes comparable with the distance between condensed counterions $\xi_c$ for $xf > u^{-2}$. This takes place along the line $\Delta f \approx xf$. In the case of weakly interacting counterions, $xf < u^{-2}$, the bead size becomes comparable with the Debye screening length $r_D$ at $\Delta f \approx u(xf)^{3/2}$. Along this line the beads size is on the order of the string thickness, leading to the uniform distribution of polymeric mass along chain's end-to-end distance. At higher effective fraction $\Delta f$ of charged monomers the chain conformation is that of an array of electrostatic blobs with size $D_e \approx (u\Delta f^2)^{-1/3}$. In Figure 3 we refer to this regime as "ordinary" polyelectrolyte regime.

Note that the poor solvent conditions for polymer backbone are not necessary for the necklace formation in the system with correlation-induced attractive interactions between condensed counterions and charged monomers. One can have a necklace structure in a Θ-solvent or even good solvent condition for the polymer backbone if the correlation-induce attractive interactions are stronger than the short-range repulsive interactions. We will consider such necklace structures and the range of its stability in future publications.

**2.2. Concentration Dependence of the Fraction of Condensed Counterions.** The dependence of the fraction of condensed counterions $x$ on polymer concentration can be obtained in the framework of the two-zone model for counterion condensation.[31] In this model the volume per chain $V_{ch} \approx N/c$ (where $c$ is the monomer concentration) is divided into two zones. The first zone is occupied by the polymer chain, the volume of which can be estimated in our case as the number of beads on the chain $N/m_b$ times the volume of a bead $D_b^3$. The second zone is the volume free of beads $V_{ch} - ND_b^3/m_b$. In a salt-free solution the total number of counterions in this volume $V_{ch}$ is equal to the total number of charged monomers on a polymer chain $fN$. The fraction $(1 - x)$ of these counterions occupies volume $V_{ch} - ND_b^3/m_b$ and is considered to be free while the fraction $x$ of these counterions is localized inside the beads. The translational part of the chain free energy associated with partitioning of counterions between two zones has the following form:

$$\frac{F_{trans}}{k_BT} \approx f(1 - x)N \ln\left[\frac{f(1 - x)cb^3}{e}\right] + fxN \ln\left[\frac{xf\rho b^3}{e}\right] \quad (29)$$

In the derivation of eq 29 we have assumed that the volume occupied by the beads $ND_b^3/m_b$ is much smaller than the volume per chain $V_{ch}$, which is true as long as the average monomer concentration $c$ is much smaller than the monomer density $\rho$ inside the beads.

Partitioning of counterions between the two zones is obtained by minimizing the total chain free energy

$$F \approx F_{neck} + F_{trans} \quad (30)$$

(where $F_{neck}$ is given by eq 24) with respect to the fraction of condensed counterions $x$. This results in the following nonlinear equation for the fraction of condensed counterions $x$

$$-\ln[(1 - x)fcb^3] + \ln[xf\rho b^3] \approx (g_p xf)^{-1} \approx \begin{cases} u^{6/5}(xf)^{3/5}, & \text{strongly correlated} \\ u^2 xf, & \text{weakly correlated} \end{cases} \quad (31)$$

where polymer density inside beads $\rho$ and the number of monomers in a polymeric correlation blob $g_p$ are given by eqs 11 and 12, respectively. In the next section we will show that this necklace model is in very good agreement with our simulation results.

## 3. Molecular Dynamics Simulations of Polyelectrolytes in Poor Solvent

**3.1. Model and Methodology.** A polyelectrolyte solution is represented in our simulation by an ensemble of $M$ chains each consisting of $N$ Lennard-Jones (LJ) monomers, with fraction $f$ of charged monomers and $N_c = fN$ counterions per chain confined into a cubic simulation box of size $L_c$ with periodic boundary conditions. We have considered polyelectrolyte chains with the following fractions of charged monomers $f = N_c/N = {}^1/_3$ (every third monomer charged), $f = {}^1/_2$ (every second monomer charged), and $f = 1$ (fully charged chain). All charged particles are monovalent ions, and therefore, the total number of charged monomers is equal to the number of counterions $MN_c$. Excluded-volume interactions between every pair of monomers are modeled by the truncated shifted Lennard-Jones (LJ) potential set to zero at the cutoff

$$U_{LJ}(r) = \begin{cases} 4\epsilon_{LJ}\left[\left(\frac{\sigma}{r}\right)^{12} - \left(\frac{\sigma}{r}\right)^6 - \left(\frac{\sigma}{r_c}\right)^{12} + \left(\frac{\sigma}{r_c}\right)^6\right] & r \le r_c \\ 0 & r > r_c \end{cases} \quad (32)$$

where the cutoff distance is equal to $r_c = 2.5\sigma$. The parameter $\epsilon_{LJ}$ controls the strength of the short-range interactions. All simulations were carried out for $\epsilon_{LJ} = 1.5k_BT$ ($k_B$ is the Boltzmann constant and $T$ is the absolute temperature), which is in the poor solvent regime far below the $\theta$-point corresponding to $\epsilon_{LJ}^{\theta} = (0.34 \pm 0.02)k_BT$ for the uncharged system.[24]

The connectivity of monomers in the chains is maintained by the finite extension nonlinear elastic (FENE) potential

$$U_{FENE}(r) = -\frac{1}{2}kR_0^2 \ln\left(1 - \frac{r^2}{R_0^2}\right) \quad (33)$$

where $k = 7\epsilon_{LJ}/\sigma^2$ is the spring constant and $R_0 = 2\sigma$ is the

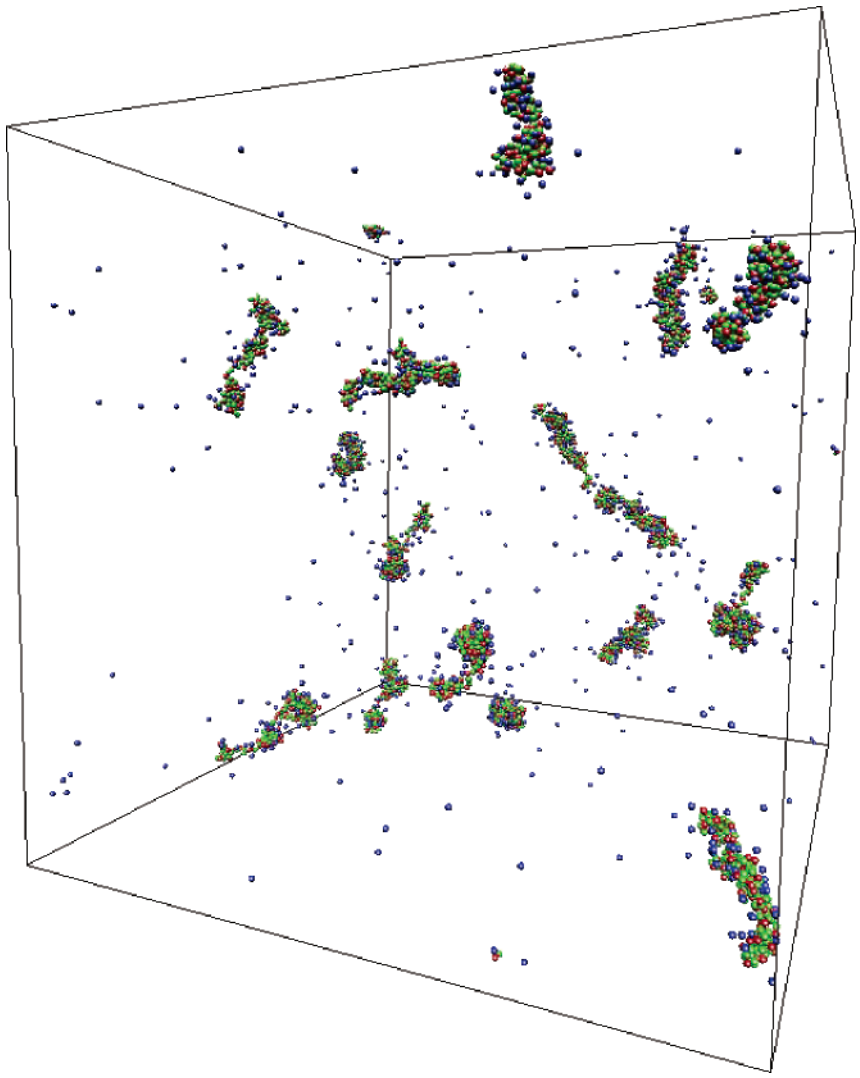

**Figure 4.** Snapshot from the simulation of a dilute polyelectrolyte solution with concentration $c = 1.5 \times 10^{-3}\sigma^{-3}$ containing 16 chains with $N = 187$ monomers and charge fraction $f = 1/3$. Counterions, charged, and neutral monomers on a chain are shown by blue, red, and green spheres, respectively.

maximum bond length at which the elastic energy of the bond becomes infinite. The FENE potential gives only the attractive part of the bond potential. The repulsive part of the bond potential is provided by the LJ interaction (eq 32).

A shifted Lennard-Jones potential is also used to describe the pure repulsive excluded-volume interactions between any pair of counterions and between a monomer and a counterion.

$$U_{\mathrm{LJ}}^{\mathrm{S}}(r) = \begin{cases} 4\epsilon_{\mathrm{LJ}}\left[\left(\frac{\sigma}{r}\right)^{12} - \left(\frac{\sigma}{r}\right)^{6}\right] + \epsilon_{\mathrm{LJ}} & r \le 2^{1/6}\sigma \\ 0 & r > 2^{1/6}\sigma \end{cases} \quad (34)$$

The parameter $\sigma$ was chosen to be the same for all monomers and counterions.

The solvent is represented by a continuum with the dielectric constant $\epsilon$. In such effective medium representation of the solvent, all charged particles interact with each other via the unscreened Coulomb potential

$$U_{\mathrm{Coul}}(r) = k_{\mathrm{B}}T\frac{l_{\mathrm{B}}q_i q_j}{r} \quad (35)$$

where $q_i$ is the charge valence of the $i$th particle equal to $+1$ for a positive charge and $-1$ for a negative charge. The Bjerrum length $l_{\mathrm{B}} = e^2/(\epsilon k_{\mathrm{B}}T)$ determines the strength of the electrostatic interactions. The electrostatic interactions between all charges in the simulation box and all their periodic images were computed by the smoothed particle mesh Ewald (SPME) algorithm[40] implemented in the DL_POLY version 2.12 software package.[41]

The molecular dynamics (MD) simulations[42] were performed by the following procedure. The initial conformations of the 16 polyelectrolyte chains in the cubic cell with periodic boundary conditions were generated as a set of self-avoiding walks. The counterions were placed randomly in the unoccupied volume of the simulation box. Both dilute and semidilute solutions of chains with the degree of polymerization $N$ varying from 25 to 373 and the value of the Bjerrum length $l_{\mathrm{B}} = 3\sigma$ were studied in the range of polymer concentrations $c$ from $1.5 \times 10^{-7}\sigma^{-3}$ to $0.15\sigma^{-3}$. The simulations were carried out at constant temperature $T = 2\epsilon_{\mathrm{LJ}}/(3k_{\mathrm{B}})$ using the Langevin thermostat. A velocity Verlet algorithm was used to integrate the equations of motion with a time step equal to $\Delta t = 0.012\tau_{\mathrm{LJ}}$. The number of MD steps was chosen large enough to allow the mean-square end-to-end distance and the mean-square radius of gyration to relax to their equilibrium values. This requirement led to the range of simulation runs between 200 000 and

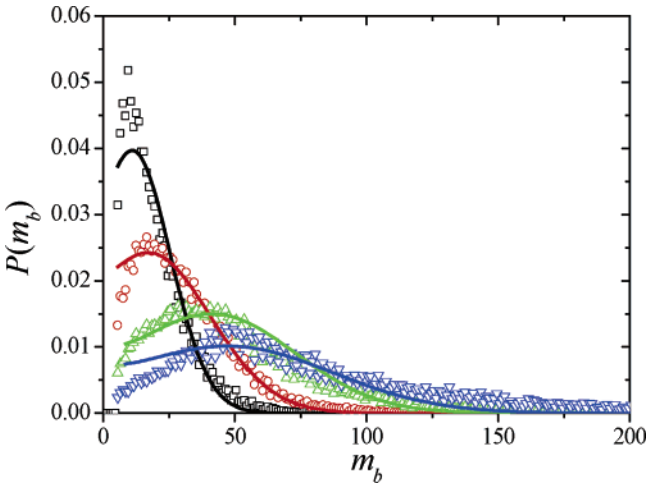


**Figure 5.** Distribution function of the number of monomers in a bead for polyelectrolyte chains with $f = 1/3$ and $N = 373$ at different polymer concentrations: $1.5 \times 10^{-6}\sigma^{-3}$ (□), $1.5 \times 10^{-5}\sigma^{-3}$ (○), $1.5 \times 10^{-4}\sigma^{-3}$ (△), and $1.5 \times 10^{-3}\sigma^{-3}$ (▽). The fitting parameters of the solid lines given by eq 39 are $\gamma = 0.336$, $m_b^* = 11$, $A = 0.0397$ for the concentration $c = 1.5 \times 10^{-6}\sigma^{-3}$; $\gamma = 0.228$, $m_b^* = 17$, $A = 0.0243$ for the concentration $c = 1.5 \times 10^{-5}\sigma^{-3}$; $\gamma = 0.399$, $m_b^* = 41$, $A = 0.0150$ for the concentration $c = 1.5 \times 10^{-4}\sigma^{-3}$; and $\gamma = 0.304$, $m_b^* = 47$, $A = 0.0101$ for the concentration $c = 1.5 \times 10^{-3}\sigma^{-3}$.

8 000 000 MD steps (2−10 relaxation times of the end-to-end vector of chains) depending on the chain length and polymer concentration.

**3.2. Dilute Solutions.** *Analysis of the Necklace Structure.* The size of a polymer chain in a dilute solution is smaller than the distance between chains. Polyelectrolytes in a poor solvent form necklace-like structures surrounded by clouds of counterions, as shown in Figure 4. The size of the necklace and the number of monomers per bead change with polymer concentration. The beads grow in size while their number decreases as polymer concentration increases.

Figure 5 shows distribution functions of the number of monomers in a bead for weakly charged chains ($f = 1/3$) at different polymer concentrations. These distribution functions were obtained by the necklace structure analysis algorithm described in detail in the Appendix. (Note that an alternative algorithm was suggested in ref 28.) At very low polymer concentration $c = 1.5 \times 10^{-6}\sigma^{-3}$ the maximum of the distribution function is located at the number of monomers in a bead $m_b \approx 12$. The peak of the distribution function shifts toward larger $m_b$ values and broadens with increasing polymer concentration while the amplitude of this peak decreases. The variations in the bead distribution function are associated with the counterion condensation. The entropic penalty for the counterion localization inside beads decreases with increasing polymer concentration $c$ resulting in the larger number of counterions residing inside beads reducing their effective charge and increasing correlation-induced attraction between counterions (see eq 31).

The analytical expression for the bead distribution function can be obtained in the regime with beads contribution dominating the necklace free energy eq 24. In this case the system of necklaces can be approximated by an ensemble of noninteracting beads. The Helmholtz free energy of the system with the total number of beads $N_{bead}$ and probability distribution $P(m_b)$ of finding a bead with $m_b$ monomers in it can be written as

$$F(P(m_b)) \approx k_B T N_{bead} \sum_{m_b} \left[ P(m_b) \left( \ln\left(\frac{P(m_b)}{e}\right) + \gamma \left( {m_b}^{2/3} + \frac{{m_b}^{5/3}}{2m_b^*} \right) - \frac{m_b}{g_p} \right) \right] \quad (36)$$

where $m_b^*$ is the optimal bead size given by eq 25. The equilibrium distribution function $P(m_b)$ is obtained by minimizing the Helmholtz free energy eq 36 with respect to $P(m_b)$ with two additional constraints, $N_{bead}\Sigma_{m_b} P(m_b) m_b =$ constant and $\Sigma_{m_b} P(m_b) = 1$, that fix the total number of monomers in all beads and normalization of the distribution function, respectively. This minimization results in the distribution function

$$P(m_b) = A \exp\left[ -\gamma m_b \left( {m_b}^{-1/3} + \frac{{m_b}^{2/3}}{2{m_b}^*} \right) + \frac{m_b}{g_p} + m_b \mu \right] \quad (37)$$

where $\mu$ is the monomeric chemical potential that determines the total number of monomers in beads and $A$ is the normalization factor. The value of the monomeric chemical potential can be analytically evaluated if the optimal beads with number of monomers $m_b^*$ provide the main contribution to the bead distribution function $P(m_b)$. Within this approximation the value of the chemical potential $\mu$ is obtained from the condition that the terms in the square brackets on the right-hand side of the eq 37 reach maximum at $m_b = m_b^*$. To satisfy this requirement, the value of the chemical potential should be equal to

$$\mu \approx 1.5\gamma (m_b^*)^{-1/3} - {g_p}^{-1} \quad (38)$$

and within this approximation the bead distribution function has the following form

$$P(m_b) \approx A \exp\left[ -\gamma m_b \left( {m_b}^{-1/3} + \frac{{m_b}^{2/3}}{2{m_b}^*} - 1.5({m_b}^*)^{-1/3} \right) \right] \quad (39)$$

This distribution function is asymmetric with respect to the maximum (the peak position), $m_b^*$. At small number of monomers in a bead, $m_b < m_b^*$, their number is controlled by the beads surface energy while for $m_b > m_b^*$ the electrostatic interactions between charged monomers prevent further bead growth. The shift of the peak position in the bead distribution function with increasing polymer concentration is consistent with the counterion condensation that reduces the effective fraction of charged monomers. The bead distribution functions are shown in Figure 5. The solid lines in Figure 5 correspond to three-parameter fits by eq 39 in which $\gamma$, $m_b^*$, and normalization factor $A$ were considered as adjustable parameters. The agreement between the simulation results and expression eq 39 (see solid lines in Figure 5) is very good.

The concentration dependence of the optimal number of monomers in a bead for chains of different lengths with fraction of charged monomers $f = 1/3$ is shown in Figure 6a. To improve statistics each point in Figure 6a is averaged over all beads with the number of monomers, $m_b$, within five monomers of the optimal bead ($m_b^* - 5 \le m_b \le m_b^* + 5$). The optimal number of monomers in a bead is independent of the chain length at low concentrations. The number of monomers in a bead has a weak dependence on polymer concentration. The growth of beads with increasing polymer concentration is an indication of the counterion condensation. The entropy loss due to the counterion localization inside and around beads decreases with

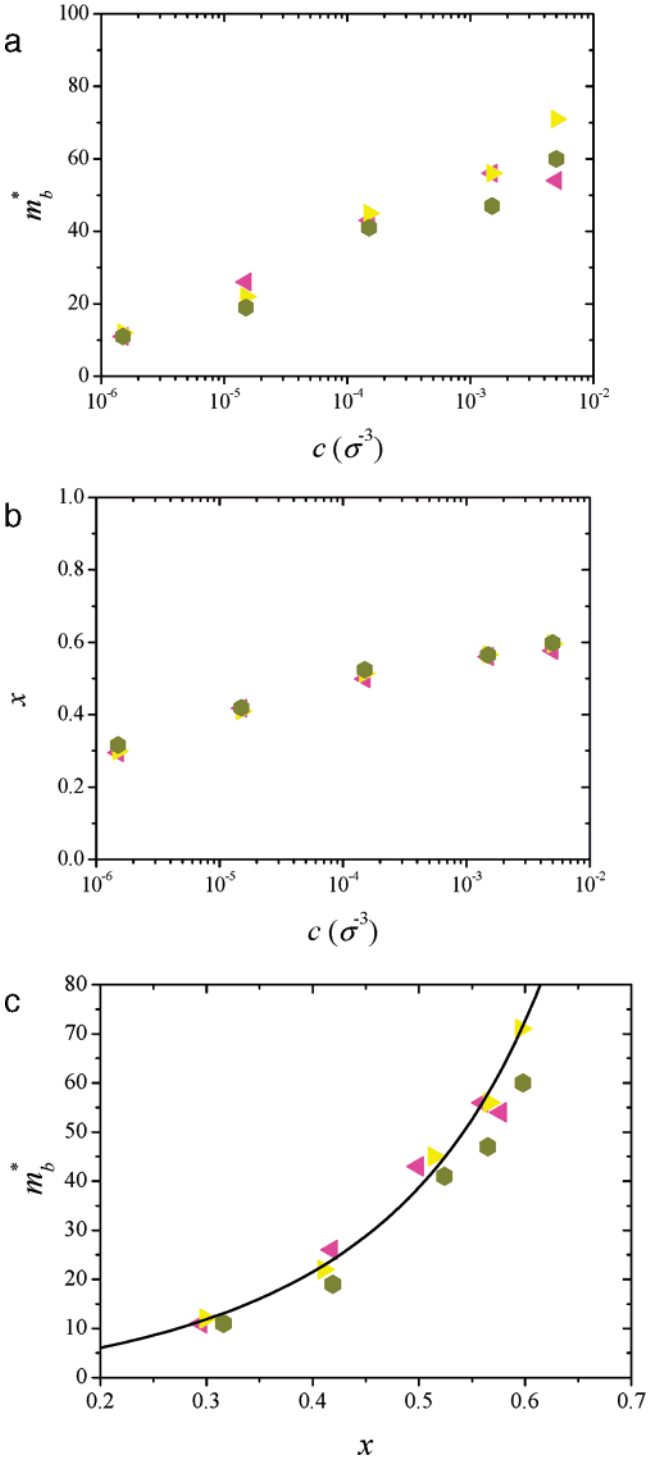


**Figure 6.** (a) Concentration dependence of the optimal number of monomers in a bead. (b) Concentration dependence of the fraction of condensed counterions, $x$. (c) Dependence of the optimal number of monomers in a bead, $m_b^*$, on the fraction of condensed counterions, $x$. Solid line is the fit to eq 40 ($m_b^* = 19.4x/(1-x)^2$) with coefficient 19.4. All three plots are for partially charged chains with fraction of charged monomers $f = 1/3$ and $N = 187$ (red triangles), 247 (yellow triangles) and 373 (hexagons).

increasing polymer concentration promoting counterion condensation. The increase of the fraction of condensed counterions with increasing concentration is demonstrated in Figure 6b. To obtain the fraction of condensed counterions for this plot, we have surrounded each monomer belonging to a bead by a sphere of radius $r_c = 1.5\sigma$ and counted all counterions with the center of mass within this cutoff distance of a monomer. The final list

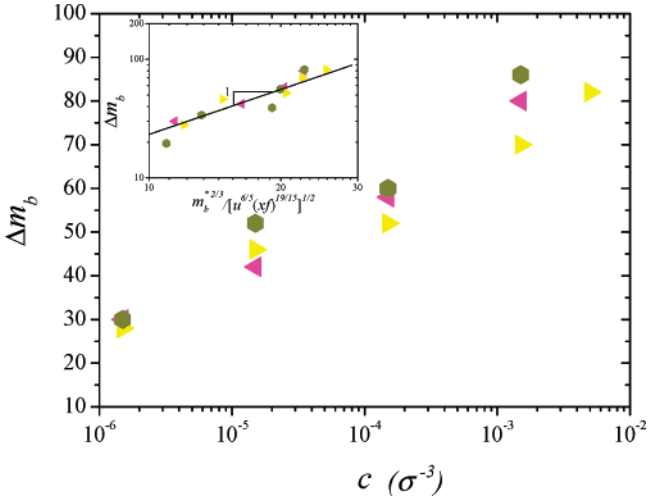


**Figure 7.** Concentration dependence of the width of the distribution function $\Delta m_b$ for weakly charged chains with $f = 1/3$ and $N = 187$ (red triangle), 247 (yellow triangle), and 373 (⬢) in dilute solution regime. Inset demonstrates universality of the dependence of $\Delta m_b$ on the parameter $m_b{}^{*2/3}/(u^{6/5}(xf)^{19/15})^{1/2}$.

of the condensed counterions was checked for multiple entries so that each condensed counterion was counted only once. The fraction of condensed counterions, $x$, is independent of the degree of polymerization $N$. Thus, the bare charge on a bead is reduced by condensed counterions at finite polymer concentrations leading to a decrease of the effective charge on a bead $(1-x)fm_b$ contributing to the bead electrostatic energy.

Equation 25 provides a very simple relation between the optimal number of monomers in a bead and the fraction of condensed counterions $x$

$$m_b{}^* \propto \frac{x}{(1-x)^2} \tag{40}$$

In Figure 6c we test this relation for weakly charged chains with the fraction of charged monomers $f = 1/3$ and different degrees of polymerization $N$ in dilute solutions. All points collapse onto one universal line (solid curve in Figure 6 c) as predicted by eq 40. This dependence confirms the fact that correlation-induced interactions between condensed counterions and charged monomers control the properties of the beads in our simulations.

The concentration dependence of the width of the bead distribution function is displayed in Figure 7. It shows broadening with increasing polymer concentration due to counterion condensation and is almost independent of the degree of polymerization. The width of the distribution function in eq 39 is estimated for the strongly correlated case as

$$\Delta m_b \approx \gamma^{-1/2} m_b{}^{*2/3} \approx m_b{}^{*2/3}/(u^{6/5}(xf)^{19/15})^{1/2} \tag{41}$$

and this dependence is tested in the inset in Figure 7. The data collapse onto one universal line with expected power law dependence. Thus, the bead distribution function eq 39 quantitatively captures the evolution of the bead size distribution with increasing polymer concentration. A similar trend in the distribution functions of the number of monomers per bead was observed for all studied chain lengths $N = 25-373$.

Figure 8 shows the distribution function of the number of beads in a necklace-like globule for polyelectrolyte chains with $N = 373$ and $f = 1/3$. At low polymer concentrations $c < 10^{-4}\sigma^{-3}$ the most probable necklace configurations are those with seven beads. As polymer concentration increases the

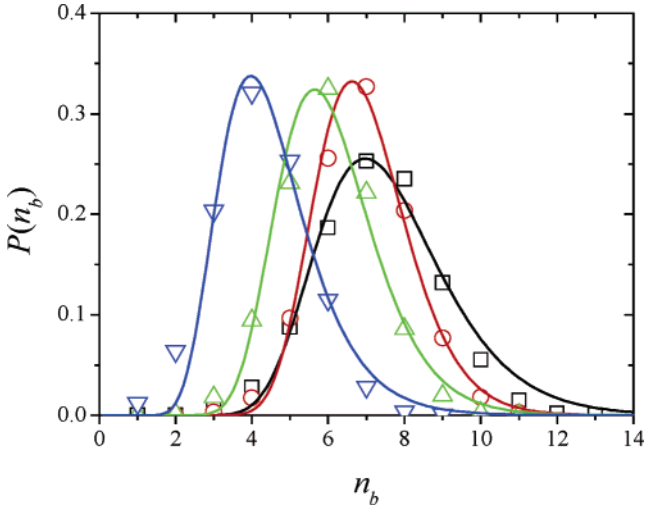


**Figure 8.** Distribution function of the number of beads per chain with $f = 1/3$ and $N = 373$ at different polymer concentrations $1.5 \times 10^{-6}\sigma^{-3}$ (□), $1.5 \times 10^{-5}\sigma^{-3}$ (○), $1.5 \times 10^{-4}\sigma^{-3}$ (△), and $1.5 \times 10^{-3}\sigma^{-3}$ (▽). The solid lines are the best fit to the equation $P(n_b) = B \exp[-C((n_b/n_b^*)^{1/3} + 0.5(n_b^*/n_b)^{2/3} - 1.5)]$. The fitting parameters of the solid lines are $C = 58.4$, $n_b^* = 6.97$, $B = 0.256$ for the concentration $c = 1.5 \times 10^{-6}\sigma^{-3}$; $C = 94.4$, $n_b^* = 6.62$, $B = 0.332$ for the concentration $c = 1.5 \times 10^{-5}\sigma^{-3}$; $C = 64.5$, $n_b^* = 5.64$, $B = 0.324$ for the concentration $c = 1.5 \times 10^{-4}\sigma^{-3}$; and $C = 39.0$, $n_b^* = 3.97$, $B = 0.338$ for the concentration $c = 1.5 \times 10^{-3}\sigma^{-3}$.

probability of the necklaces with $n_b > 5$ decreases while necklaces with four beads become more favorable. They appear in the system with higher probability at polymer concentration around $c \approx 1.5 \times 10^{-3}\sigma^{-3}$.

We can write down the distribution function of the number of beads per chain if the free energy of the beads controls necklace free energy. In this case the energy of the necklace is on the order of the energy of individual beads times the number of beads per chain $n_b$ and the distribution function of the number of beads per chain becomes

$$P(n_b) \approx B \exp\left[-n_b\gamma\left(m_b^{2/3} + \frac{m_b^{5/3}}{2m_b^*}\right) + 1.5\gamma n_b^*(m_b^*)^{2/3}\right]$$

$$\approx B \exp\left[-\frac{\gamma N_b}{(m_b^*)^{1/3}}\left(\left(\frac{n_b}{n_b^*}\right)^{1/3} + \frac{1}{2}\left(\frac{n_b^*}{n_b}\right)^{2/3} - \frac{3}{2}\right)\right] \quad (42)$$

where $B$ is the normalization factor and $N_b = m_b n_b$ is the number of monomers in all beads. In eq 42 the energy of the necklace with $n_b$ beads is measured with respect to the energy of the optimal necklace with $n_b^*$ beads and each bead consisting of $m_b^*$ monomers. In writing the distribution function (eq 42), we assumed that the optimal number of beads per chain is equal to $n_b^* = N_b/m_b^*$. The width of this distribution function narrows as the number of monomers in beads $N_b$ increases. For narrow distribution the average number of beads per chain is on the order of the optimal number of beads $n_b^*$. The solid lines in Figure 8 correspond to eq 42 in which parameter $\gamma N_b/(m_b^*)^{1/3}$, normalization factor $B$, and the optimal number of beads per chain $n_b^*$ are considered to be adjustable parameters. As one can see from Figure 8, the lines corresponding to theoretically predicted distribution function (eq 42) are in excellent agreement with the simulation data.

The shift of the distribution function of the number of beads per chain with increasing polymer concentration toward smaller $n_b$ indicates that the bead's growth occurs at the expense of other beads and strings. This is further corroborated by Figure 9, depicting the concentration dependence of the average number of beads per chain for polyelectrolytes with $f = 1/3$ (a) and $f = 1/2$ (b). In the case of weakly charged chains with $f = 1/3$, the average number of beads per chain monotonically decreases with increasing polymer concentration. This decrease becomes less pronounced in the concentration range close to polymer overlap. However, the average number of beads per chain for stronger charged polyelectrolytes with $f = 1/2$ first slightly increases with the concentration in the dilute regime due to the fact that the chains are strongly stretched, and the fraction of monomers in strings is much larger than that in beads at very low concentrations. Small beads are formed from the monomers of strings with increasing concentration in the case of stronger charged chains, while small beads are merged into large beads as polymer concentration increases in the case of weaker charged chains. This can also be a mechanism of the bead nucleation and growth.

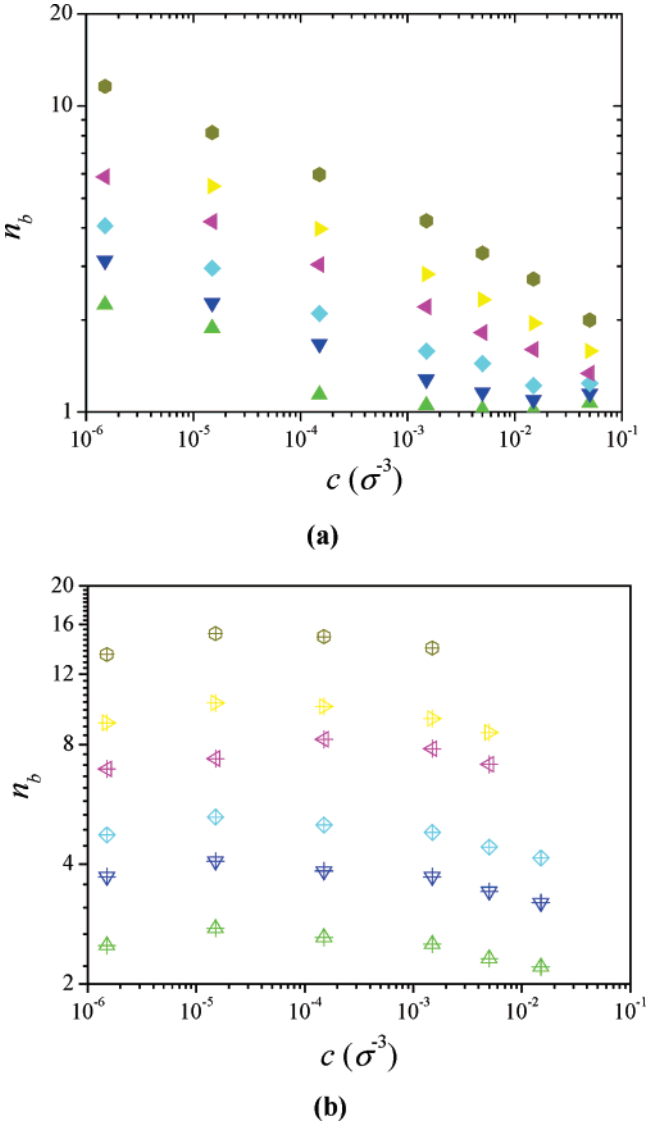


**Figure 9.** Dependence of the average number of beads per chain on polymer concentration for chains with (a) $N = 61$ (green triangle), 94 (purple triangle), 124 (blue square), 187 (red triangle), 247 (yellow triangle), 373 (●) for $f = 1/3$ and (b) $N = 61$ (crossed green triangle), 94 (crossed purple triangle), 124 (crossed blue rhomb), 187 (crossed red triangle), 247 (crossed yellow triangle), 373 (crossed hexagon).

In the previous section we argued that the stretching of the necklace is controlled by the effective charge of the cylinder with thickness $l_{str}$ surrounding the necklace. In particular, eq

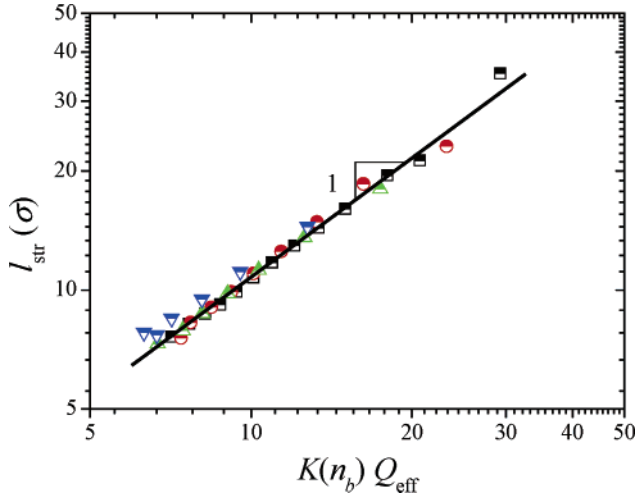


**Figure 10.** Relation between the string length and effective charge per one bead and one string for polymer chains with $f = 1/3$ and $N = 247$. $c = 1.5 \times 10^{-6}\sigma^{-3}$ (half-filled black squares), $1.5 \times 10^{-5}\sigma^{-3}$ (half-filled red circles), $1.5 \times 10^{-4}\sigma^{-3}$ (half-filled green triangles), and $1.5 \times 10^{-3}\sigma^{-3}$ (half-filled blue inverse triangles).

26 gives the linear relation for the distance between the centers of mass of the neighboring beads $l_{str}$ and the effective charge $Q_{eff}$. To verify this relation, Figure 10 shows a universal plot of the dependence of the average distance between the centers of mass of two neighboring beads $l_{str}$ on the factor $Q_{eff}K(n_b)$ (see eqs 26−28). All data for necklaces with $f = 1/3$ and different number of beads per chain existing at different polymer concentrations collapse reasonably well into one universal plot. The slope of this universal line is close to unity as predicted by eq 26. The effective charge per string $Q_{eff}$ was estimated in our simulations in the following way. First, all consecutive centers of mass of beads were connected by straight lines. This operation leads to a coarse-grained model of the necklace—the polymer chain of beads. The polymer backbone of this polymer chain of beads was surrounded by a set of overlapping spherical shells of radius $l_{str}/2$ (about 10 per each string). The counterions occupying the selected volume were counted. It is important to point out that during this procedure each counterion was counted only once. The effective charge $Q_{eff}$ was obtained by dividing the net charge of the selected object (the bare charge of the polymer chain minus the net charge of counterions) by the total number of beads. The linear charge density of the necklace partially screened by counterions $l_B Q_{eff}/l_{str}$ is still above the threshold value of unity corresponding to the counterion condensation.

*Necklace Form Factor.* Small-angle neutron scattering (SANS) and small-angle X-ray scattering (SAXS) techniques can be used to analyze the necklace structure. In dilute solutions the scattering is dominated by the single chain contribution, and both techniques measure the single chain form factor

$$P_{intra}(q) = \frac{1}{N^2}\langle \sum_{i,j} \exp(i\vec{q}\cdot\vec{r}_{ij})\rangle = \frac{1}{N^2}\left\langle \sum_{i,j} \frac{\sin(qr_{ij})}{qr_{ij}} \right\rangle \quad (43)$$

where $\vec{q}$ is the wave vector, $\vec{r}_{ij}$ is the vector between $i$th and $j$th monomers on the chain, and brackets $\langle\ \rangle$ denote ensemble average over all possible chain conformations.

Figure 11 shows the single chain form factor obtained from our simulations. As one can see from this figure, all features that one would expect to observe for the scattering from the necklace-like chains are smoothened out by the variations in the necklace structures between necklaces with different number of beads. The oscillations in the chain form factor at large $q$ correspond to the length scales on the order of a bond length and are due to correlations between positions of neighboring monomers along the polymer backbone.

To extract the information about bead size from the chain form factor, one can use the Kratky plot.[20,21] Figure 12 a shows the Kratky plot of $q^2P_{intra}(q)$ vs $q$ at different polymer concentrations for chains with the degree of polymerization $N = 247$ and fraction of charged monomers $f = 1/3$. The function $q^2P_{intra}(q)$ has a local maximum in the range of the wavenumbers

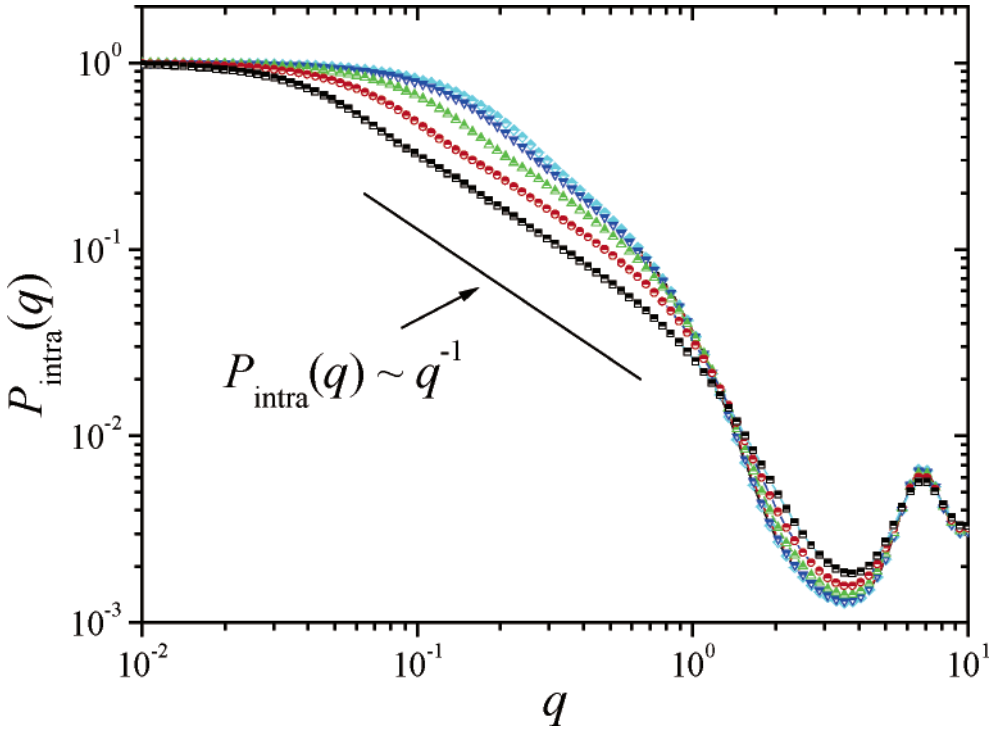


**Figure 11.** Form factor of polyelectrolyte chain in a dilute solution for chains with degree of polymerization $N = 247$ and fraction of charged monomers $f = 1/3$ at polymer concentrations $c = 1.5 \times 10^{-6}\sigma^{-3}$ (half-filled black squares), $1.5 \times 10^{-5}\sigma^{-3}$ (half-filled red circles), $1.5 \times 10^{-4}\sigma^{-3}$ (half-filled green triangles), $1.5 \times 10^{-3}\sigma^{-3}$ (half-filled blue inverse triangles), and $5.0 \times 10^{-3}\sigma^{-3}$ (half-filled light blue rhombs), respectively.

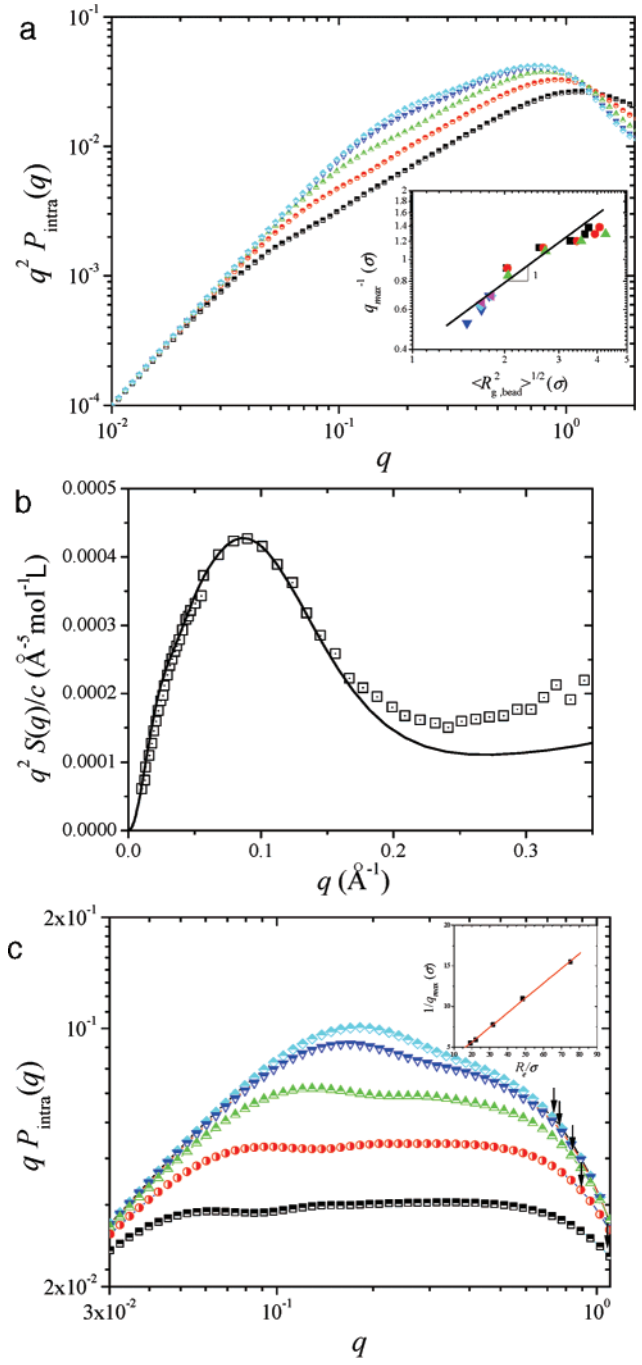


**Figure 12.** (a) Kratky plot of the form factor of partially charged chains with $f = {}^1/_3$ and with the degree of polymerization $N = 247$ at $c = 1.5 \times 10^{-6}\,\sigma^{-3}$ (half-filled black squares), $1.5 \times 10^{-5}\sigma^{-3}$ (half-filled red circles), $1.5 \times 10^{-4}\sigma^{-3}$ (half-filled green triangles), $1.5 \times 10^{-3}\sigma^{-3}$ (half-filled blue inverse triangles), and $5.0 \times 10^{-3}\sigma^{-3}$ (half-filled light blue rhombs). Inset: dependence of $q_{max}^{-1}$ on the bead radius of gyration $\langle R_{g,bead}^2\rangle^{1/2}$ for different polymer concentrations. **(**b) Comparison of simulation data with experiments for Kratky plot of the form factor of a polyelectrolyte chain. Solid line shows the simulation results for partially charged chains with $f = {}^1/_3$ and with the degree of polymerization $N = 247$ at polymer concentration $c = 5 \times 10^{-3}\sigma^{-3}$. Squares are experimental data of Spiteri and Boue (see text for details). (c) Holtzer plot of the form factor of polyelectrolyte chains with degree of polymerization $N = 247$ and fraction of charged monomers $f = {}^1/_3$ at different concentrations $c = 1.5 \times 10^{-3}\sigma^{-6}$ (half-filled black squares), $1.5 \times 10^{-5}\sigma^{-3}$ (half-filled red circles), $1.5 \times 10^{-4}\sigma^{-3}$ (half-filled green triangles), $1.5 \times 10^{-3}\sigma^{-3}$ (half-filled blue inverse triangles), and $5.0 \times 10^{-3}\sigma^{-3}$ (half-filled light blue rhombs). Arrows point to the locations of maximum on the corresponding Kratky's plot associated with the bead size (see (a)). Location of the low $q$ maximum correlates well with the chain size (see inset).

$q < 1$. The maximum becomes less pronounced, and its position moves toward larger $q$ values as polymer concentration decreases. It can be barely distinguished at polymer concentration $c = 1.5 \times 10^{-6}\sigma^{-3}$. The concentration dependence of the maximum indicates that it can be associated with the bead size. To verify that the maximum in $q^2P_{intra}(q)$ is correlated with the beads, we show in the inset the dependence of the $q_{max}^{-1}$ on the bead size $\langle R_{g,bead}^2\rangle^{1/2}$ for chains of different lengths and fraction of charge monomers. The data points closely follow the straight line with unit slope. The deviation of the points from the straight line is due to relatively close location of the peak to the minimum on the Kratky plot which is due to correlation between neighboring along the polymer backbone monomers which influences the position of the maximum.

Figure 12b shows superposition of the Kratky plot of $q^2P_{intra}(q)$ at polymer concentration $c = 5 \times 10^{-3}\sigma^{-3}$ for chains with the degree of polymerization $N = 247$ and fraction of charged monomers $f = {}^1/_3$ with experimental Kratky plot $q^2S(q)/c$ of Spiteri and Boue on 36% sulfonated NaPSS mixture of hydrogenated polystyrene with molar mass 68 kDa (with the degree of polymerization $N = 487$) and deuterated polystyrene with molar mass 73 kDa.[21] In the original figure by Spiteri and Boue the maximum of the $q^2S(q)/c$ function is located at $q = 0.085$ Å$^{-1}$ and is equal to $4.3 \times 10^{-4}$ Å$^{-5}$ mol$^{-1}$ l. To combine simulation and scattering data, we use rescaling along the $q$-axes of the simulation graph by factor $a = 0.085/0.724 = 0.12\sigma$ Å$^{-1}$ to superimpose the positions of corresponding $q_{max}$ and along $q^2S(q)/c$ axes by the factor $\lambda = 4.3 \times 10^{-4}/0.042 = 0.01\sigma^2$ Å$^{-5}$ mol$^{-1}$ l to superimpose magnitudes of the peaks. As one can see, the shape of the maximum is almost identical in both systems.

To display the deviation of the chain form factor from that of a rodlike chain, we use Holtzer plot $qP_{intra}(q)$ vs $q$ (see Figure 12c). For a rodlike chain this plot levels off at the value of the wave vector $q$ of the order of $2\pi/R_e$, where $R_e$ is the chain length. In the case of the necklace the Holtzer plot shows additional oscillation. These oscillations are associated with the correlations in the beads locations along the polymer backbone. The first maximum in this plot corresponds to correlation between monomers belonging to two beads located at the ends of polyelectrolyte chain. With increasing polymer concentration the magnitude of this peak increases while it position shifts toward larger $q$ values. This shift is a result of the counterion condensation on the beads which leads to increase in their size and shrinkage of the polyelectrolyte chain. To verify that this peak is indeed due to correlations between monomers belonging to the last two beads in the inset to Figure 12c, we demonstrate the linear dependence of the $q_{max}^{-1}$ on the chain size $R_e$.

*Osmotic Coefficient.* Figure 13 presents the concentration dependence of the osmotic coefficient of necklaces, defined as the ratio of the solution osmotic pressure $\pi$ to the ideal mixture osmotic pressure $k_BTcf$ of all counterions. The osmotic coefficient $\phi$ first decreases with increasing polymer concentration $c$ and then starts to increase as polymer concentration approaches chain overlap. This behavior of the osmotic coefficient is similar to that reported for polyelectrolytes in the Θ-solvent case. In our previous publication[43] we have shown that the osmotic coefficient $\phi$ of the dilute polyelectrolyte solution can be approximated by that obtained in the framework of the two-zone model[44]

$$\phi_{dilute} \approx \frac{\gamma_R}{\gamma_0}\left(1 - B\frac{cR_e(c)^3}{N}\right)^{-1} \qquad (44a)$$

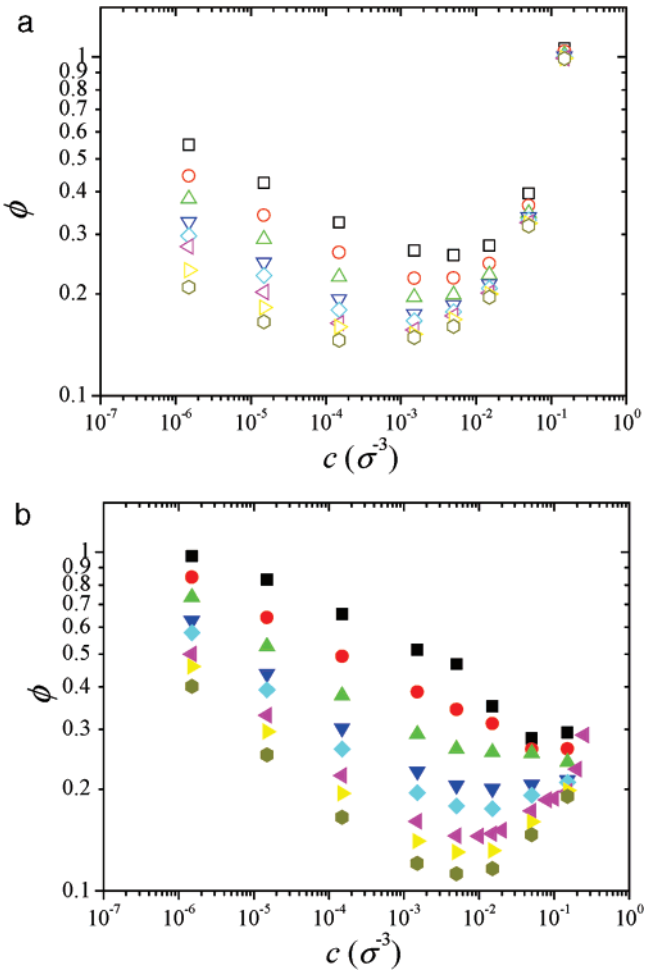


**Figure 13.** (a) Concentration dependence of the osmotic coefficient for fully charged chain with $f = 1$. $N = 25$ (□), 40 (red ○), 61 (green △), 94 (purple ▽), 124 (blue ◇), 187 (red △), 247(yellow △), 373 (⬡). (b) Concentration dependence of the osmotic coefficient for partially charged chain with $f = 1/3$. $N = 25$ (■), 40 (red ●), 61 (green ▲), 94 (purple ▼), 124 (blue ◆), 187 (red ▲), 247 (yellow ▲), 373 (⬢).

where $\gamma_0$ is the reduced linear charge density $\gamma_0 = Ql_B/R_e$ on the macroion ($R_e$ is the average end-to-end distance of the macroion), $\gamma_R$ is the reduced linear charge density $\gamma_R = Q_R l_B/R_e$ of the cylindrical region around macroion with radius $R_e/2$, and $B$ is the numerical coefficient on the order of unity. To apply the two-zone model to the dilute solution of necklaces, one has to keep in mind that the distribution of the electrostatic potential around the necklace has cylindrical symmetry at length scales $l_{str}/2 < r < R_e/2$ from the axis of the necklace. In this case the reduced linear charge density $\gamma_0$ is equal to $Q_{eff}l_B/l_{str}$ because the counterions distributed inside the spherical region around beads with radius $l_{str}/2$ reduce the bare charge of the polyelectrolyte chain.

To verify the predictions for the osmotic coefficient in dilute solutions given by the eq 44a, Figure 14 shows the universal plot of the reduced osmotic coefficient $\gamma_0\phi/\gamma_R$ as a function of the ratio of polymer concentration $c$ to monomer concentration within the cylindrical region $c[R_e(c)]^3/N$. The solid line is given by eq 44a with the parameter $B = 1.95$. All data points for polyelectrolyte chains with fraction of charged monomers $f = 1$ and $1/2$ and for larger chains with $f = 1/3$ collapsed onto one universal curve. However, the data for shorter weakly charged polyelectrolytes with $f = 1/3$ slightly deviate from this universal curve. This deviation is due to the lack of cylindrical symmetry for short necklaces with very few large beads. For the necklace

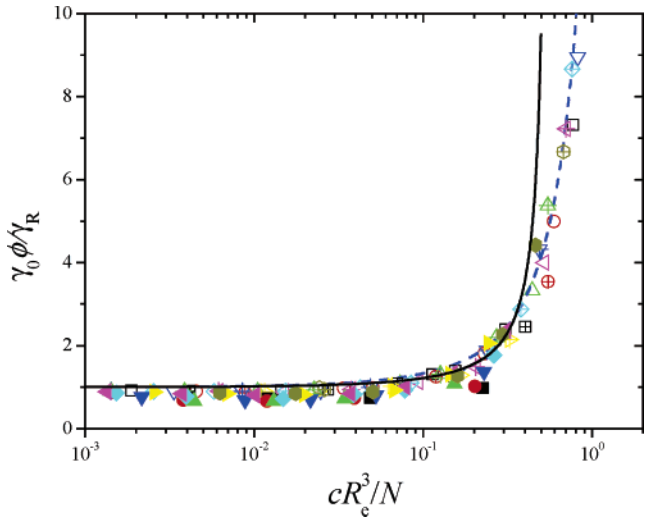


**Figure 14.** Universal plot of $\gamma_0\phi/\gamma_R$vs normalized polymer concentration. $f = 1$: $N = 25$ (□), 40 (red ○), 61 (green △), 94 (▽), 124 (◇), 187 (red △), 247 (yellow △), 373 (⬡); $f = 1/2$: $N = 25$ (⊞), 40 (red ⊕), 61 (green crossed △), 94 (crossed ▽), 124 (crossed ◇), 187 (red crossed △), 247 (yellow crossed △), 373 (crossed ⬡); $f = 1/3$: $N = 25$ (■), 40 (red ●), 61 (green ▲), 94 (purple ▼), 124 (blue ◆), 187 (red ▲), 247 (yellow ▲), 373 (⬢). The solid line corresponds to the equation $(\gamma_0\phi_{dilute}/\gamma_R) \approx [1 - 1.95(cR_e(c)^3/N)]^{-1}$ and the dashed line $\gamma_0\phi_{dilute}/\gamma_R \approx \exp[2.85(cR_e(c)^3/N)]$.

with large beads the counterion distribution has a spherical symmetry up to the length scales of the order of the distance between beads. There is very small region with cylindrical-like symmetry on length scales between $l_{str}$ and $R_e$ for necklaces with small number of beads.

We can improve the agreement with the simulation data approximating the osmotic coefficient by an empirical function

$$\phi_{dilute} \approx \frac{\gamma_R}{\gamma_0} \exp\left(B_e \frac{cR_e(c)^3}{N}\right) \qquad (44b)$$

This equation is shown in Figure 14 as a dashed line. Both functions are close at low polymer concentrations while exponential function fits simulation data better in concentration rage close to the chain overlap.

**3.3. Semidilute Solutions.** *Overlap Concentration.* Polyelectrolyte chains begin to overlap when the distance between them becomes on the order of their size. The important difference between solutions of necklaces and polyelectrolyte solutions in good or Θ-solvent is that solutions of necklaces has broad distribution of necklaces in size and number of beads per chain. A single globular chain coexists with necklace-like chains with different number of beads at the same concentration (see Figure 8). Such high polydispersity of sizes can significantly influence the $N$ dependence of the overlap concentration. Figure 15 presents the $N$ dependence of the overlap concentration. The overlap concentration of polyelectrolytes with low charge density ($f = 1/3$) has very weak $N$ dependence for short chains ($N < 94$). This is due to the fact that short polyelectrolytes form a globular conformation near the overlap concentration with roughly the same concentration $\rho$ inside the globule independent of the chain length. Overlap of such globules occurs at the same concentration on the order of the concentration $\rho$ inside globules. For longer chains with $N = 94$, 124 and $f = 1/3$ the preferential conformation of a polyelectrolyte chain is a dumbbell. However, for the longest chains with $N = 187$, 247, 372 and $f = 1/3$ there are more than three beads on the necklace at the overlap concentration. We conclude that polyelectrolytes in our simula-

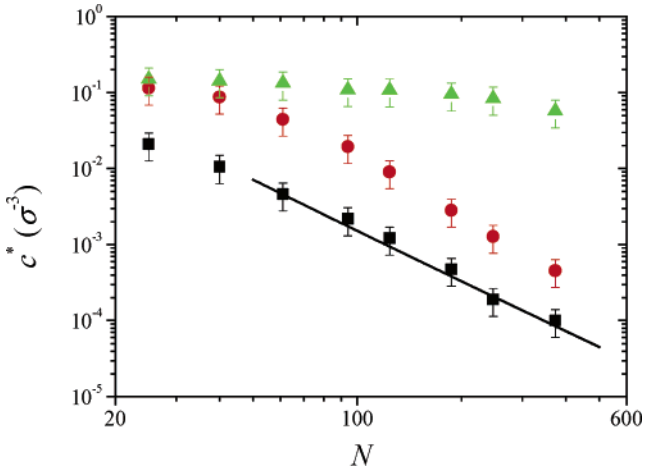


**Figure 15.** Dependence of the overlap concentration on the number of monomers $N$. $f = 1$ (■), $^1/_2$ (●), and $^1/_3$ (▲).

tions are too short to see the universal behavior of the chain overlap concentration. All our data correspond to a crossover between solutions containing bead-like aggregates (globules) and necklace-like chains.

For stronger charged chains with $f = {}^1/_2$ the overlap concentration decreases faster with polymer concentration. This is due to the fact that for stronger charged chains with $f = {}^1/_2$ there are more beads per chain at the overlap concentration than in the case of weaker charged chains with $f = {}^1/_3$. In the case of fully charged chains ($f = 1$) the electrostatic repulsion is always stronger than the Lennard-Jones attraction, and there are only very small beads with fewer than five monomers. Structure of polyelectrolytes with such small aggregates is similar to that of a chain in Θ- or good solvents for polymer backbone. Therefore, the overlap concentration of fully charged chains exhibits the strongest decrease with chain degree of polymerization $N$ and falls in the concentration range reported for simulations of polyelectrolyte in a Θ-solvent regime.[45] In this case the relation between the number of monomers $N$ and the overlap concentration $c^*$ can be estimated as

$$c^* \propto N^{-2} \ln^{-1}(N/g_e) \tag{45}$$

where $g_e$ is the number of monomers in the electrostatic blob (for fully charge chains it is on the order of unity). The solid line in Figure 15 corresponds to eq 45. The dependence of the overlap concentration $c^*$ for fully charged chains ($f = 1$) on the chain degree of polymerization $N$ follows the scaling relation predictions (eq 45) for longer chains but deviates from it for shorter chains. A similar trend was observed in our simulations of polyelectrolytes in a Θ-solvent regime (see for details refs 43 and 45) and was attributed to the finite size effect.

*Correlation Length and Chain Size.* The important length scale above the overlap concentration, $c > c^*$, is the correlation length $\xi$—the average mesh size of the semidilute polyelectrolyte solutions. For semidilute solution of polyelectrolyte chains in a Θ- or good solvent for polymer backbone the correlation length $\xi$ is inversely proportional to the square root of polymer concentration ($\xi \sim c^{-1/2}$).[46] Scaling theory[18,19] predicts two different regimes in the dependence of the correlation length on polyelectrolyte concentration in poor solvents due to the two different length scales (the string length and the bead size). The correlation length has the same concentration dependence as in semidilute polyelectrolyte solutions in Θ- or good solvents for polymer backbone if there are many beads per correlation volume. The crossover to a new concentration regime is

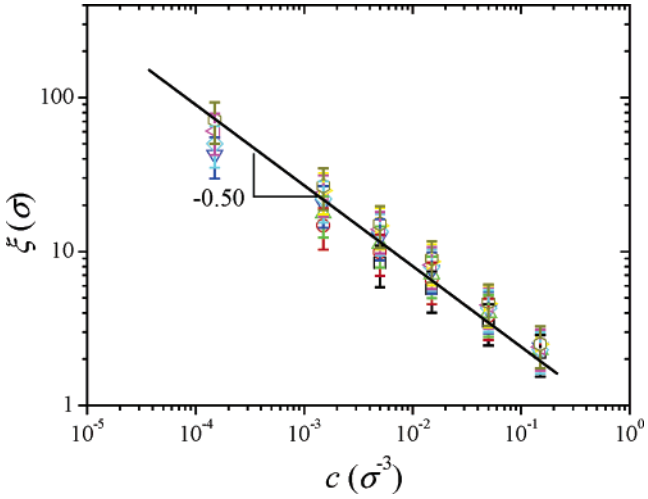


**Figure 16.** Concentration dependence of the correlation length for fully charged chains $f = 1$: $N = 25$ (□), 40 (red ○), 61 (green △), 94 (purple ▽), 124 (blue ◇), 187 (red △), 247 (yellow △), 373 (⬡).

expected at the polymer concentration at which the distance between two neighboring beads along the polymer backbone becomes comparable with the correlation length $\xi$. At higher polymer concentrations there will be on average one bead per each correlation volume, and such a solution can be described as a dilute solution of beads. The correlation length in dilute solutions is inversely proportional to the cubic root of polymer concentration ($\xi \sim c^{-1/3}$).

To evaluate the correlation length $\xi$ in our simulations, we use the monomer−monomer pair correlation function $g(r)$. This correlation function $g(r)$ is proportional to the probability of finding a pair of monomers at distance $r$ from each other. The pair correlation function consists of the intermolecular and the intramolecular contributions

$$g(r) = g_{\text{inter}}(r) + g_{\text{intra}}(r) \tag{46}$$

The intramolecular correlation function is defined as

$$g_{\text{inra}}(r) = \frac{1}{cMN}\left\langle \sum_{n=1}^{M}\sum_{i=1}^{N}\sum_{j=1}^{N} \delta(\vec{r} - \vec{r}_{ij}^{\,nn}) \right\rangle \tag{47}$$

The intermolecular contribution to the pair correlation function is the sum over all pairs of molecules $m$ and $n$ (out of $M$ chains in the system) and over all pairs of monomers on these molecules

$$g_{\text{inter}}(r) = \frac{1}{cMN}\left\langle \sum_{n\neq m=1}^{M}\sum_{i=1}^{N}\sum_{j=1}^{N} \delta(\vec{r} - \vec{r}_{ij}^{\,nm}) \right\rangle \tag{48}$$

where $\vec{r}_{ij}^{\,nm}$ is the vector between $i$th and $j$th monomers on the chains $n$ and $m$, respectively. We define the correlation length $\xi$ as the length scale at which these intra- and intermolecular contributions to the pair correlation function are equal. At this distance $\xi$ from a monomer on a given chain one can find with equal probability monomers belonging to the same or different chains (see ref 45 for details).

Figure 16 shows the concentration dependence of the correlation length in semidilute solutions. The usual concentration dependence of the correlation length is seen in Figure 16 for data representing fully charged chains with $f = 1$. Fully charged chains do not form necklaces in semidilute solutions. The slope of the concentration dependence of the correlation length for fully charged chains ($f = 1$) approaches the scaling value $-{}^1/_2$

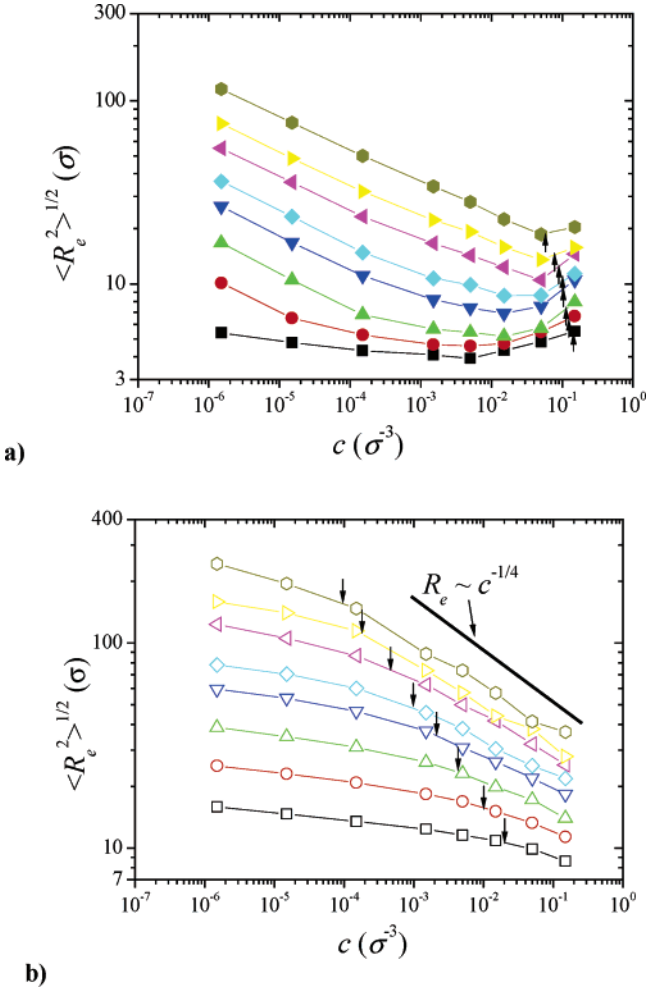


**Figure 17.** Concentration dependence of the chain size for chains with (a) $f = 1/3$: $N = 25$ (■), 40 (red ●), 61 (green ▲), 94 (purple ▼), 124 (blue ◆), 187 (red ▲), 247 (yellow ▲), 373 (⬢), and (b) $f = 1$: $N = 25$ (□), 40 (red ○), 61 (green △), 94 (purple ▽), 124 (blue ◇), 187 (red △), 247 (yellow △), 373 (⬡). The locations of the overlap concentration $c^*$ are marked by the arrows.

(see Figure 16). However, there is an $N$ dependence of the correlation length (similar to the one reported for polyelectrolytes in a Θ-solvent). The correlation length increases with increasing number of monomers $N$ on the chain. For longer chains this increase is less pronounced and almost completely disappears for our longest chains with $N = 187$, 247, and 373 monomers. This $N$ dependence of the correlation length is due to the finite size effects that dominate properties of shorter chains and are suppressed for longer chains as was demonstrated for polyelectrolytes in a Θ-solvent.[45] Unfortunately, we do not have enough data points in semidilute regime to establish concentration dependence of the correlation length for polyelectrolyte chains with $f = 1/3$.

The chain size of weakly charged polyelectrolytes with fraction of charged monomers $f = 1/3$ exhibits nonmonotonic dependence on polymer concentration (see Figure 17a). It decreases at low polymer concentrations and increases at high polymer concentrations. The decrease at low concentrations is due to increasing fraction of condensed counterions that screen electrostatic repulsion and increase correlation-induced attraction. For short polyelectrolyte chains ($N < 94$) the minimum in the concentration dependence of chain size is located in a dilute solution regime. The swelling of polyelectrolytes in a dilute solution at concentrations higher than this minimum can be explained by one more effect of counterion condensation. In our simulations the short-range interactions between monomers and counterions are purely repulsive (see eq 34). Thus, the condensed counterions could not only lead to the collapse of polyelectrolytes by reducing their effective charge but also to the swelling of already collapsed globules when there is a sufficient number of counterions inside globules. In some sense counterions play the role of a cosolvent for polymer backbone leading to chain swelling with increasing polymer concentration due to increasing fraction of the condensed counterions. For longer polyelectrolyte chains ($N > 124$) the increase in the chain size takes place at polymer concentration at which the beads start to overlap.

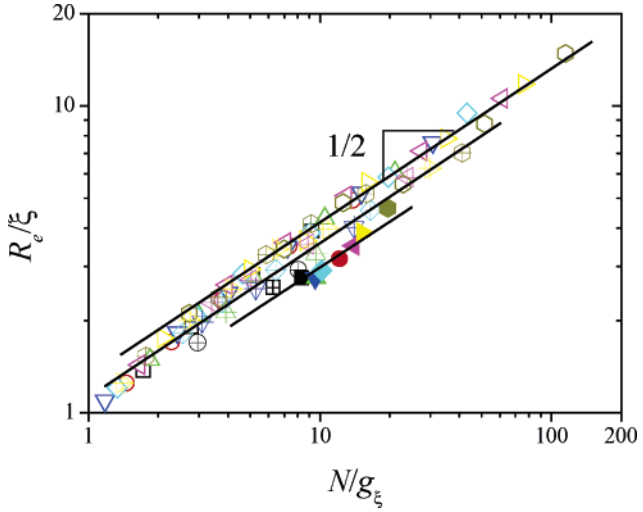


**Figure 18.** Dependence of the reduced chain size $R_e/\xi$ on the number of correlation blobs $N/g_\xi$ for chains with different degrees of polymerization, fraction of charged monomers, and at different polymer concentrations. $f = 1$: $N = 25$ (□), 40 (red ○), 61 (green △), 94 (purple ▽), 124 (blue ◇), 187 (red △), 247 (yellow △), 373 (⬡); $f = 1/2$: $N = 25$ (⊞), 40 (red ⊕), 61 (green crossed △), 94 (purple crossed ▽), 124 (blue crossed ◇), 187 (red crossed △), 247 (yellow crossed △), 373 (crossed ⬡); $f = 1/3$: $N = 25$ (■), 40 (red ●), 61 (green ▲), 94 (▼), 124(◆), 187 (red ▲), 247 (yellow ▲), 373 (⬢). Thin solid lines have slope $1/2$.

The usual monotonic concentration dependence of the chain size in polyelectrolyte solutions of fully charged chains ($f = 1$) is shown in Figure 17b. The chain size decreases with increasing polymer concentration. The decrease of the chain size is associated with the screening of the intrachain electrostatic repulsion by counterions and by other polyelectrolyte chains. According to the scaling hypothesis,[46,47] a polyelectrolyte chain in semidilute solution is assumed to be flexible at length scales on the order of the correlation length $\xi$. Thus, the size of the polyelectrolyte chain is that of a Gaussian chain consisting of $N/g_\xi$ Kuhn segments with length on the order of $\xi$ (where $g_\xi$ is the number of monomers per correlation length).

$$R_e \approx \xi\left(\frac{N}{g_\xi}\right)^{1/2} \propto N^{1/2}c^{-1/4} \tag{49}$$

Figure 18 shows the plot of $R_e/\xi$ vs $N/g_\xi$. All three data sets collapse onto their corresponding "universal" curves with slope $1/2$. Thus, there is a systematic shift between "universal" curves corresponding to different fractions $f$ of charged monomers. The deviation from the single universal scaling line could be explained by the presence of beads on the chains. For chains with low fractions of charged monomers the beads are bigger, and the number of correlation blobs per chain is not sufficient to achieve the scaling limit.

## 4. Summary

We have developed a necklace model of hydrophobic polyelectrolytes in which the correlation-induced attractive interactions between condensed counterions are the leading factors determining the chain collapse and bead formation. According to this model, the beads grow in size with increasing polymer concentration while their number per chain decreases. The strong fluctuations in the number of monomers per bead leads to coexistence of necklaces with different number of beads per chain at any polymer concentration. To test the predictions of this new necklace model, we performed molecular dynamics simulations of salt-free polyelectrolyte solutions in a poor solvent for polymer backbone. Polyelectrolytes were modeled as chains of charged and neutral Lennard-Jones particles connected by the finite extension nonlinear elastic potential bonds. In these simulations we have studied several ensembles of chains with degrees of polymerization $N = 25-373$ and fractions of charged monomers $f = {}^1/_3$, ${}^1/_2$, and 1. The electrostatic interactions between all species in the system were taken into account by the smoothed particle mesh Ewald method.

Our simulations confirmed that partially charged chains (with $f = {}^1/_2$ and ${}^1/_3$) form necklace-like structures of beads and strings in dilute solutions. However, for half-charged chains ($f = {}^1/_2$) the beads are relatively small, and such necklace structures correspond to a crossover between polyelectrolyte and necklace regimes in the diagram of states (Figure 3). The optimal number of monomers in a bead is determined by the Rayleigh stability condition that is the result of the optimization of the correlation-induced attractive interactions between condensed counterions controlling the bead surface energy and electrostatic repulsion between uncompensated charged monomers occupying the bead. The number of monomers in a bead grows with increasing polymer concentration (see Figure 6a). The number of monomers per bead is determined exclusively by the intrabead interactions since points for different chain lengths collapse onto one universal line at low concentration. The deviation from the universality appears if the number of monomers in a bead becomes comparable with the total number of monomers per chain $N$. The bead growth is an indication of the counterion condensation. More counterions are localized inside the bead with increasing polymer concentration, reducing its effective charge and increasing the correlation-induced attraction. The dependence of the optimal number of monomers $m_b^*$ on the fraction $x$ of condensed counterions (eq 40) is universal and independent of the chain degree of polymerization (see Figure 6c).

There is a linear relationship between the length of the string connecting two neighboring beads and the effective charge of the cylinder with diameter equal to the string length (see Figure 10). The counterions distributed inside this cylinder reduce the strength of the electrostatic interaction between charges shortening strings. The balance between interbead electrostatic interactions and the correlation-induced attraction between condensed counterions determines the equilibrium string length.

The strong variations in the chain structure in dilute solutions (the coexistence of the necklaces with different number of beads) hide the information about the bead size and string length in the chain form factor $P_{intra}(q)$ (see Figure 11). The existence of beads is shown in this form factor as a small bump in the region with $q$ near unity. The necklace structure of chains is observed by the Kratky plot of $q^2P_{intra}(q)$ vs $q$ of the form factor with the peak corresponding to scattering from beads (see Figure 12a). The Kratky plot obtained in our simulations is in excellent agreement with data of neutron scattering experiments. The reciprocal wave vector $1/q_{max}$ of the maximum in the Kratky plot is proportional to the bead size shifts as shown in the inset in Figure 12a.

The Holtzer plot $qP_{intra}(q)$ vs $q$ for the necklace-like chains (see Figure 12c) exhibits oscillations. These oscillations are associated with the correlations in the beads locations along the polymer backbone. The first maximum in this plot corresponds to correlation between monomers belonging to two beads located at the ends of polyelectrolyte chain. With increasing polymer concentration the magnitude of this peak increases while it position shifts toward larger $q$ values. This shift is consistent with the counterion condensation leading to the reduction of the electrostatic repulsion between beads and to the decrease in the chain size.

The fully charged chains with $f = 1$ do not form necklaces in dilute solutions for the temperature $T = 2\epsilon_{LJ}/(3k_B)$. In this case the electrostatic repulsion is too strong to allow local chain collapse. All our results for necklace structures in dilute solutions are in a good qualitative agreement with the results of the molecular dynamic simulations by Limbach and Holm.[28]

Crossover from a dilute to a semidilute regime occurs at polymer concentrations at which the distance between chains becomes comparable to the chain size. In our simulations we determined the overlap concentrations by comparing the root-mean-square end-to-end distance with the average distance between the centers of mass of neighboring chains. The simulation data for $N$ dependence of the overlap concentration $c^*$ for strongly charged chains ($f = 1$ and ${}^1/_2$) approaches the scaling law $N^{-2}\ \ln^{-1} N$ as the degree of polymerization $N$ increases (see Figure 15). However, for chains with the fraction of charged monomers $f = {}^1/_3$ there is a very weak $N$ dependence of the overlap concentration on the chain degree of polymerization. Thus, all our systems correspond to a crossover between globular aggregates (single beads) and necklace-like chains.

The correlation length $\xi$ in semidilute solutions is defined as a length scale at which the intra- and interchain contributions to the total monomer−monomer correlation function are equal to each other.[45] In semidilute solutions we found that there is a weak dependence of the correlation length on the chain degree of polymerization $N$. This $N$ dependence of the correlation length $\xi$ is more pronounced for shorter chains but almost disappears for the set of our longest chains. Thus, such $N$ dependence can be associated with finite size effects (similar $N$ dependence of the correlation length was reported for polyelectrolytes in Θ-solvents). In the system of short chains the contribution of the chain ends is comparable to that from the middle of the chain, leading to a noticeable $N$ dependence. For fully charged chains the exponent for concentration dependence of the correlation length is close to $-{}^1/_2$, in agreement with the scaling model (see Figure 16).

The osmotic coefficient exhibits nonmonotonic dependence on the polymer concentration for all solutions in our study (see Figure 13). In dilute solutions the osmotic coefficient of polyelectrolyte chains decreases with increasing polymer concentration. This concentration dependence of the osmotic coefficient is proportional to the fraction of counterions distributed outside of the volume of polyelectrolyte chains ($\phi \sim \gamma_R/\gamma_0$, see Figure 14). With increasing polymer concentration

the fraction of counterions within the chain volume increases, leading to the reduction of the net charge of the cylindrical region and the corresponding reduction of the chain size. Polyelectrolyte chains contract with increasing polymer concentration (see Figure 17 a,b), and the effective linear charge density on them increases leading to further counterion condensation. Our results show that the two-zone model[44] is capable of capturing the correct concentration dependence of the osmotic coefficient independently of the details of chain structure. The universal plot shown in Figure 14 works reasonably well for chains with all fractions of charged monomers investigated ($f = 1$, $^1/_2$, and $^1/_3$).

**Acknowledgment.** The authors are grateful to the National Science Foundation for the financial support under Grants CHE-9876674 (M.R), ECS-0103307 (M.R.), DMR-0305203 (A.V.D.), NASA, under Grant NCC-1-02037 (M.R.). Q. L. is grateful for the support from the National Natural Science Foundation of China under Grant 20474075.

## Appendix

To carry out a quantitative analysis of our simulation data, we need a reliable algorithm that will allow us to separate monomers into those belonging to beads and monomers belonging to strings. Our algorithm is based on the fact that the monomers in a bead are crowded having more nearest neighbors than monomers in a string. The sorting of monomers between beads and strings begins with determination of the number of the nearest neighbors for each monomer within a sphere of radius $R_{cut}$. The selected monomer was considered to be inside the initial bead cluster if the number of surrounding monomers within the sphere of radius $R_{cut}$ was larger than $n_{clust}$. Otherwise, it was assigned to a string. An index 1 was assigned to all monomers inside clusters and index 0 to those in strings. After this first pass we start combining monomers into beads and strings. Since all our monomers are connected into polymer chain and beads and strings are formed by consecutive monomers along polymer backbone, we simply cluster together all sequences of ones and zeros along the polymer backbone. Figure 19 shows the process of cluster analysis for a conformation of a polyelectrolyte chain with $N = 187$ in a dilute solution at concentration $c = 1.5 \times 10^{-4}\sigma^{-3}$. The initial cluster assignment is shown in Figure 19a where monomers belonging to dense clusters with the typical number of nearest neighbors $n_{clust} > 8$ within cutoff distance $R_{cut} = 2\sigma$ are colored in red and monomers assigned to initial strings and loops are shown in white color. As one can see the initial sorting algorithm overassigns monomers to strings and loops. The loop is a string of monomers that begins and ends at the same bead. The loops are usually formed by sequences of monomers located on the bead surface which have smaller number of nearest neighbors than monomers inside beads. To eliminate loops, we search the nearest-neighbors lists for a monomer belonging to two consecutive clusters separated by a loop. If lists contain repetitive entries, these two initial clusters are merged into one including monomers forming the connecting loop. The process of loop elimination continues until the cluster structure does not change after two consecutive passes. The final result for the cluster analysis after completion of the loop elimination process is presented in Figure 19b. This process successfully eliminated all initial loops of monomers located on the surface of the final beads, confirming the robustness of the algorithm described above.

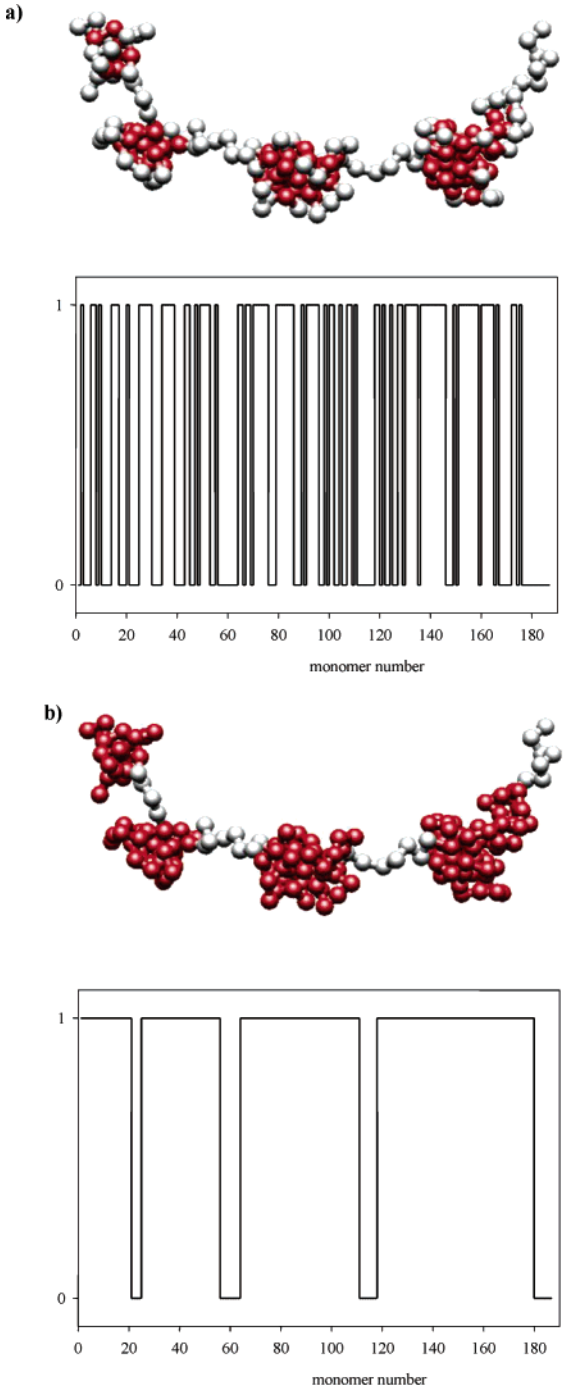


**Figure 19.** Bead−string analysis for a polyelectrolyte chain with $N = 187$ monomers and charge fraction $f = ^1/_3$ in a dilute solution with polymer concentration $c = 1.5 \times 10^{-4}\sigma^{-3}$. (a) Initial cluster assignment for $n_{clust} = 8$ nearest neighbors within a cutoff distance $R_{cut} = 2\sigma$. Monomers belonging to clusters are colored in red, and monomers assigned to initial strings and loops are shown in white color. (b) Final result of the cluster analysis after the elimination of loops.

## References and Notes

(1) Grosberg, A. Y.; Khokhlov, A. R. *Statistical Physics of Macromolecules;* AIP Press: New York, 1994.
(2) Rubinstein, M.; Colby, R. H. *Polymer Physics*; Oxford University Press: New York, 2003.
(3) Katchalsky, A.; Eisenberg, H. *J. Polym. Sci.* **1951**, *6*, 145−154.
(4) Morawetz, H. *J. Polym. Sci., Part B: Polym. Phys.* **2002**, *40*, 1080−1086.

(5) Hooper, H. H.; Beltran, S.; Sassi, A. P.; Blanch, H. W.; Prausnitz, J. M. *J. Chem. Phys.* **1990**, *93*, 2715−2723.
(6) Higgs, P. G.; Orland, H. *J. Chem. Phys.* **1991**, *95*, 4506−4518.
(7) Rayleigh, L. *Philos. Mag.* **1882**, *14*, 184.
(8) Dobrynin, A. V.; Rubinstein, M.; Obukhov, S. P. *Macromolecules* **1996**, *29*, 2974−2979.
(9) Chodanowski, P.; Stoll, S. *J. Chem. Phys.* **1999**, *111*, 6069−6081.
(10) Lyulin, A. V.; Dunweg, B.; Borisov, O. V.; Darinskii, A. A. *Macromolecules* **1999**, *32*, 3264−3278.
(11) Solis, F. J.; de la Cruz, M. O. *Macromolecules* **1998**, *31*, 5502−5506.
(12) Balazs, A. C.; et al. *Prog. Surf. Sci.* **1997**, *55*, 181−269.
(13) Migliorini, G.; Lee, N.; Rostiashvili, V.; Vilgis, T. A. *Eur. Phys. J. E* **2001**, *6*, 259−270.
(14) Aseyev, V. O.; Klenin, S. I.; Tenhu, H.; Grillo, I.; Geissler, E. *Macromolecules* **2001**, *34*, 3706−3709.
(15) Lee, M. J.; Green, M. M.; Mikes, F.; Morawetz, H. *Macromolecules* **2002**, *35*, 4216−4217.
(16) Kiriy, A.; et al. *J. Am. Chem. Soc.* **2002**, *124*, 13454−13462.
(17) Minko, S.; Kiriy, A.; Gorodyska, G.; Stamm, M. *J. Am. Chem. Soc.* **2002**, *124*, 3218−3219.
(18) Dobrynin, A. V.; Rubinstein, M. *Macromolecules* **1999**, *32*, 915−922.
(19) Dobrynin, A. V.; Rubinstein, M. *Macromolecules* **2001**, *34*, 1964−1972.
(20) Essafi, W. Thesis, 1996.
(21) Spiteri, M. N. Thesis, 1997.
(22) Heitz, C.; Rawiso, M.; Francois, J. *Polymer* **1999**, *40*, 1637−1650.
(23) Waigh, T. A.; Ober, R.; Williams, C. E.; Galin, J. C. *Macromolecules* **2001**, *34*, 1973−1980.
(24) Micka, U.; Holm, C.; Kremer, K. *Langmuir* **1999**, *15*, 4033−4044.
(25) Micka, U.; Kremer, K. *Europhys. Lett.* **2000**, *49*, 189−195.
(26) Limbach, H. J.; Holm, C.; Kremer, K. *Europhys. Lett.* **2002**, *60*, 566−572.
(27) Limbach, H. J.; Holm, C. *Comput. Phys. Commun.* **2002**, *147*, 321−324.
(28) Limbach, H. J.; Holm, C. *J. Phys. Chem. B* **2003**, *107*, 8041−8055.
(29) Limbach, H. J.; Holm, C.; Kremer, K. *Macromol. Symp.* **2004**, *211*, 43−53.
(30) Ulrich, S.; Laguecir, A.; Stoll, S. *J. Chem. Phys.* **2005**, *122*, 094911-1−094911-9.
(31) Oosawa, F. *Polyelectrolytes*; Marcel Dekker: New York, 1971.
(32) Schiessel, H.; Pincus, P. *Macromolecules* **1998**, *31*, 7953−7959.
(33) Schiessel, H. *Macromolecules* **1999**, *32*, 5673−5680.
(34) Grosberg, A. Y.; Nguyen, T. T.; Shklovskii, B. I. *Rev. Mod. Phys.* **2002**, *74*, 329−345.
(35) Levin, Y. *Rep. Prog. Phys.* **2002**, *65*, 1577−1632.
(36) de Gennes, P. G. *Scaling Concepts in Polymer Physics;* Cornell University Press: Ithaca, NY, 1979.
(37) Shklovskii, B. I. *Phys. Rev. Lett.* **1999**, *82*, 3268−3271.
(38) Brilliantov, N. V.; Kuznetsov, D. V.; Klein, R. *Phys. Rev. Lett.* **1998**, *81*, 1433−1436.
(39) Dobrynin, A. V.; Colby, R. H.; Rubinstein, M. *J. Polym. Sci., Part B: Polym. Phys.* **2004**, *42*, 3513−3538.
(40) Essman, U.; Perera, L.; Berkovitz, M. L. *J. Chem. Phys.* **1995**, *103*, 8577.
(41) Forester, T. R.; Smith, W. *The DL_POLY_2 Reference Manual*; Daresbury Laboratory, Daresbury, 2000.
(42) Frenkel, D.; Smit, B. *Understanding Molecular Simulations*; Academic Press: San Diego, 2001.
(43) Liao, Q.; Dobrynin, A. V.; Rubinstein, M. *Macromolecules* **2003**, *36*, 3399−3410.
(44) Deshkovski, A.; Obukhov, S.; Rubinstein, M. *Phys. Rev. Lett.* **2001**, *86*, 2341−2344.
(45) Liao, Q.; Dobrynin, A. V.; Rubinstein, M. *Macromolecules* **2003**, *36*, 3386−3398.
(46) de Gennes, P.-G.; Pincus, P.; Brochard, F.; Velasco, R. M. *J. Phys. (Paris)* **1976**, *37*, 1461−1476.
(47) Dobrynin, A. V.; Colby, R. H.; Rubinstein, M. *Macromolecules* **1995**, *28*, 1859−1871.

MA052086S